Available online at www.sciencedirect.com
SCIENCE DIRECT
ELSEVIER
Diabetes Research and Clinical Practice 73 (2006) 135–142
DIABETES RESEARCH AND CLINICAL PRACTICE
www.elsevier.com/locate/diabres

Role of hepatic AMPK activation in glucose metabolism and dexamethasone-induced regulation of AMPK expression

Amelia Y.I. Viana [a,b], Hideyuki Sakoda [c], Motonobu Anai [d], Midori Fujishiro [c], Hiraku Ono [d], Akifumi Kushiyama [c], Yasushi Fukushima [c], Yuzo Sato [e], Yoshiharu Oshida [a], Yasunobu Uchijima [b], Hiroki Kurihara [b], Tomoichiro Asano [b,*]

[a] *Department of Sports Medicine, Graduate School of Medicine, Nagoya University, 65 Tsurumai-cho, Showa-ku, Nagoya 466-8550, Japan*
[b] *Department of Physiological Chemistry and Metabolism, Graduate School of Medicine, University of Tokyo, 7-3-1 Hongo, Bunkyo-ku, Tokyo 113-8655, Japan*
[c] *Department of Internal Medicine, Faculty of Medicine, University of Tokyo, 7-3-1 Hongo, Bunkyo-ku, Tokyo 113-8655, Japan*
[d] *The Institute for Adult Diseases, Asahi Life Foundation, Tokyo 160-0023, Japan*
[e] *Department of Health Science, Faculty of Psychological and Physical Science, Aichi Gakuin University, Nisshin 470-0195, Japan*

Received 15 February 2005; received in revised form 30 May 2005; accepted 21 December 2005
Available online 28 February 2006

Abstract

To elucidate the role of AMPK in hepatic glucose metabolism, dominant negative (DN), constitutively active (CA) forms of the AMPKα1 subunit and control vector LacZ were overexpressed by means of adenovirus-mediated gene transfer. Five days after virus injection, hepatic AMPK activity was five-fold higher in CA mice than in DN mice. DN mice were apparently glucose intolerant with a higher fasting plasma glucose level (DN 82.3 ± 0.7 mg/dl, CA 42.5 ± 4.8 mg/dl and LacZ 54.3 ± 2.4 mg/dl). PEPCK, a gluconeogenic key enzyme, mRNA was increased 131.54% and 48.92% in DN mice compared to that of CA and LacZ, respectively. Thus, hepatic AMPK activation plays a role in the suppression of gluconeogenesis and this might be the cause of decreased fasting plasma glucose level in CA mice.

We also investigated the effects of dexamethasone on hepatic AMPK expression and activity in rat liver, mice liver, as well as primary cultured hepatocytes. Subcutaneously injecting mice with dexamethasone (1 mg/day) for 5 days significantly upregulated hepatic AMPKα1 and α2 expressions. Similarly, the treatment of primary cultured rat hepatocytes with dexamethasone (1 μM) increased expression of the AMPKα1 subunit, AICAR-induced AMPK phosphorylation and kinase activity.

Although increased AMPK expression cannot be attributed to dexamethasone-induced glucose intolerance, taken together our results raise the possibility that AMPK control liver glucose output and its expression in liver might be modulated by various hormones and growth factors.

Keywords: AMPK; AICAR; Glucose metabolism; Dexamethasone; Insulin resistance

1. Introduction

The activations of PI 3-kinase/Akt and AMP-activated protein kinase (AMPK) are reportedly involved in GLUT4 translocation in response to insulin

* Corresponding author. Tel.: +81 3 3815 5411x33133; fax: +81 3 5803 1874.
E-mail address: asano-tky@umin.ac.jp (T. Asano).

0168-8227/$ – see front matter © 2006 Elsevier Ireland Ltd. All rights reserved.
doi:10.1016/j.diabres.2005.12.011

and muscle contraction, respectively [1–4]. Activation of AMPK also induces the phosphorylation and inactivation of acetyl-CoA carboxylase, decreasing malonyl-CoA and thereby relieving inhibition of carnitine palmytoil-transferase (CPT-1) and allowing an increase in fatty acid oxidation [5,6]. Thus, the actions of AMPK appear to be designed to prevent ATP depletion by promoting glucose uptake into muscle fibers, and lipid catabolism in the liver [7,8].

On the other hand, the role of AMPK in hepatic glucose metabolism is still unclear. Previous studies [9–11] suggest that stimulation with 5-aminoimidazole-4-carboxamide ribonucleoside (AICAR), an activator of AMPK, inhibits fatty acid synthase (FAS), L-type pyruvate kinase (PK), spot 14 (S-14) genes involved in the conversion of carbohydrates to lipids in the liver, and both glucose 6-phosphatase (G6Pase) and phosphoenolpyruvate (PEPCK), key enzymes of gluconeogenesis, responsible for the biosynthesis of glucose from non-carbohydrate precursors. However, AICAR is not a highly specific activator of AMPK [12]. We thus overexpressed constitutively active (CAα1) and dominant negative (DNα1) forms of AMPKα1 using recombinant adenoviruses to investigate the role of AMPK in regulating key enzymes of glucose metabolism.

Next, we investigated whether glucocorticoids affect the expression and kinase activity of hepatic AMPK. Glucocorticoids reportedly induce insulin resistance and their clinical use often exacerbates diabetes mellitus [13,14], but to date there are no reports on the regulation of AMPK by dexamethasone. Thus, our study is the first one to reveal the effect of dexamethasone in regulating expressions of AMPKα1 and α2 and their kinase activities, in mouse liver and primarily cultured hepatocytes.

Herein, we show that in vivo AMPK activation leads to decreases in gluconeogenesis, promoting a reduction in hepatic glucose output and consequent blood glucose levels. In addition, the AMPK protein expression is increased by dexamethasone treatment, which raises the possibility that various hormones and growth factors also modulate hepatic glucose and lipid metabolic processes via altered AMPK expression.

2. Materials and methods

2.1. Materials

Dexamethasone was purchased from Sigma (St. Louis, MO, USA). All other reagents from commercial sources were of analytical grade.

2.2. Antibodies

An antibody against the AMPKα subunit was prepared by immunization of rabbits with a GST-rat AMPKα2 subunit fusion protein. The antibodies raised against AMPKα were then affinity purified, as previously described [15]. Anti-α1, anti-α2 and anti-phospho-AMPK-Thr172 were purchased from Upstate Biotechnology Inc. (Lake Placid, NY).

2.3. Rats and mice

Four-week-old male SD rats and C57BL/6 mice were fed a standard rodent diet. Some rats received subcutaneous dexamethasone injection (1 mg/day) for 5 days. Food was withdrawn for 12 h, the rats were anesthetized with pentobarbital sodium (60 mg/kg body weight i.p.), and the liver dissected out.

2.4. Hepatocytes

Hepatocytes were isolated from male Sprague–Dawley (SD) rats (Tokyo Experimental Animals, Tokyo, Japan), weighing 180–200 g, by the collagenase method [16]. Cells were suspended in William's E medium (Sigma), containing 10% fetal bovine serum (FBS), 1 nM insulin, 75 mg/l penicillin and 50 mg/l streptomycin, and then plated. After 12 h, the cells were made serum free and divided into control or dexamethasone (1 μM) groups. The medium was the same as that described above except that 0.1% BSA was added instead of FBS. The cells were incubated in dexamethasone for 12 or 24 h, at which point the medium was changed to Krebs Ringer bicarbonate (KRB) buffer with 8 mM glucose. After 1 h, AICAR (500 μM) was added. Cells were harvested 1 h after starting the AICAR incubation.

2.5. Generation of recombinant adenoviruses

The cDNA encoding residues 1–312 of AMPKα1, containing a mutation that alters threonine 172 to an aspartic acid (T172D), was generated and its recombinant adenovirus produced, as descried previously [17]. The cDNA encoding AMPKα1, containing a mutation that alters threonine residue 172 to alanine, was used to construct DNα1. Both constructs were designed to contain a c-*myc* tag at the NH_2 terminus. Adenovirus expressing LacZ were used as control group. The amplified adenoviruses were purified and concentrated using cesium chloride ultracentrifugation. The resultant viruses were then dialyzed into phosphate-buffered saline containing 10% glycerol.

2.6. Gene transfer to murine liver

Male C57BL/6 mice (8–10 weeks of age) were injected, via the tail vein, with adenovirus at a dose of 2.5×10^7 plaque-forming units/g body weight. Animals were fasted for 16 h

before blood sampling, and then sacrificed. Blood glucose was measured with a portable blood glucose monitor, Glutest-Ace (Sanwa Kagaku Kenkyusho, Nagoya, Japan). Serum triglyceride and cholesterol were assayed as previously described [18].

2.7. AMPK assay

The assay of AMPK activity was performed as described previously [12].

2.8. Immunopreciptation and immunoblotting

The supernatants from hepatocytes and liver lysates were boiled in Laemmli sample buffer containing 100 mmol/l DTT. SDS-PAGE and Western blotting were performed as described previously [12], with anti-AMPKα1, α2 and anti-phospho-AMPK-Thr172.

2.9. RNA preparation

Total cell RNA was isolated from hepatocytes, rat muscle and liver using an Isogen RNA isolation kit (Nippon Gene, Tokyo). RNA concentrations were estimated based on absorbance at 260 nm, and 10 μg of RNA from each sample was used for the RNase protection assay described below.

2.10. Preparation of riboprobes

To obtain rat AMPKα1 and α2 cDNA, PCR was performed based on reported sequences obtained from rat cDNA libraries. The amplified fragments, which corresponded to nucleotides 1450–1647 and 1398–1662 of rat AMPKα1 and α2 cDNA, respectively, were subcloned using pBluescript II SK minus, after which the resultant plasmids were linearized with *Xba*I. The mouse PEPCK (196–395), G6Pase (601–800), GK (1133–1304), PFK (826–985) and PK (1591–1856) cDNAs were also obtained as described above.

2.11. RNase protection assay

RNase protection assays were carried out according to the manufacturer's instructions (RPA III; Ambion, Austin, TX). Pooled 10 μg samples of total RNA were hybridized with the above riboprobes. After treatment with RNase, the protected fragments were resolved on 5% polycrylamide-urea gels and subjected to autoradiography. The intensities of the resultant bands were then determined using a Molecular Imager GS-525.

2.12. Statistical analysis

Results are expressed as means ± S.E. Comparisons were made using the unpaired Student's *t*-test. Values of $P < 0.05$ were considered statistically significant.

3. Results

3.1. Overexpression of constitutively active and dominant negative AMPKα1 in murine liver

Adenovirus-mediated overexpressions of CAα1 and DNα1 were detected by immunoblotting using the antibody against the myc-tag (Fig. 1A). Since CAα1 is a truncated mutant of AMPKα1, it was detected as a band at a smaller molecular weight than the endogenous subunit (Fig. 1B). On the other hand, DNα1 is slightly larger than endogenous AMPKα1 due to attachment of the myc-tag in DNα1 (Fig. 1B). While the overexpression of CAα1 did not affect the amount of endogenous AMPKα1 (data not shown), overexpressing DNα1 markedly decreased the amount of endogenous AMPKα1, as has already been reported [12,19]. This is considered to be because the free form of AMPKα1 is degraded far more rapidly than the combined form of AMPKα1 with β and γ subunits. Consequently, the amounts of CAα1 and DNα1 in each mouse were approximately four- to six-fold those of the respective endogenous AMPKα1.

Next, the kinase activity of AMPKα in the liver was measured. As shown in Fig. 1C, the AMPKα kinase activity in DNα1 was shown to be decreased to less than 20% of that in CAα1 mice.

3.2. The effects of constitutively active and dominant negative AMPKα1 on glucose metabolism

Glucose tolerance testing of LacZ, CAα1 and DNα1 mice was performed (Fig. 2). Fasting plasma glucose levels were significantly higher on DNα1 (82.3 ± 0.7 mg/dl) compared to that of LacZ (54.3 ± 2.4 mg/dl) and CAα1 (42.5 ± 4.8 mg/dl), and 15 min after glucose injection, blood glucose values were 324.7 mg/dl for DNα1, 155.8 mg/dl for CAα1 and 250.0 mg/dl for LacZ mice (Fig. 2). Thus, DNα1 mice were found to be glucose resistant in comparison with LacZ and CAα1 mice.

The effects of overexpressions of LacZ, DNα1 and CAα1 viruses on the expression levels of the key enzymes for gluconeogenesis and glycolysis were assessed using RNase protection assay (Fig. 3). PEPCK mRNA, a key enzyme of gluconeogenesis, was decreased 131.54% in CAα1 and 48.92% in LacZ, as compared to that of DNα1 mice (Fig. 3A). There was no significant difference in G6Pase, another key gluconeogenesis enzyme, upon comparison of mRNA levels in the two groups (Fig. 3B).

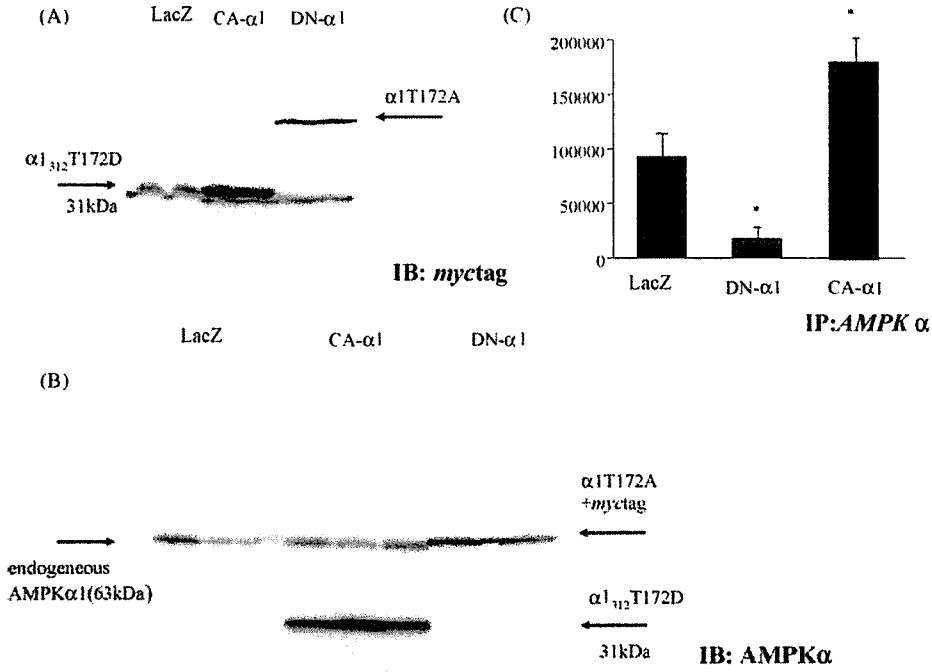

Fig. 1. Expressions of dominant negative and constitutively active forms of AMPKα1 subunit in murine liver. (A) Samples were immunoblotted with anti-myc antibody. (B) Immunoblotted with AMPKα1. Decreased endogenous AMPKα1 protein content in DN mice. (C) AMPK activity was increased five-fold in CA as compared to DN mice. Samples were immunopreciptated with AMPKα1 antibody and AMPK activity in the immune complexes was measured as a function of phosphorylation of SAMS peptide ($^{*}P < 0.01$).

Moreover, a key glycolysis enzyme, glucokinase, was decreased 49.8% in CAα1 mice, comparing to that of DN mice. Glucokinase was also 44.0% decreased in DNα1 mice if compared to that of LacZ (Fig. 3C). There was no significant difference in the phosphofructokinase or the pyruvate kinase mRNA level (Fig. 3D and E).

3.3. Effects of dexamethasone treatment on the AMPK expression in rat liver and mice liver

To investigate its in vivo effect, dexamethasone was given to the rats as a daily subcutaneous injection (1 mg/day) for 5 days. Rat livers were subjected to immunoblot analysis and RNase protection assay. AMPKα1 protein content (Fig. 4A) and mRNA levels (Fig. 4B) were apparently increased by 2- and 2.5-fold, respectively, in the livers of rats treated with dexamethasone for 5 days. Hepatic AMPKα2 protein content (Fig. 4C) and mRNA levels (Fig. 4D) were also increased in dexamethasone treated rats. In mice, AMPKα1 was increase by 1.9-fold (Fig. 4E) and AMPKα2 by 1.6-fold (Fig. 4F) if compared to that of control group following the same dexamethasone treatment.

3.4. Effect of dexamethasone incubation on hepatocytes

Subsequently, primary cultured hepatocytes were incubated with 1 μM dexamethasone for 12 and 24 h, and immunoblot analyses of lysates from these hepatocytes were carried out. As shown in Fig. 4G and H, dexamethasone treatment promoted a significant increase in AMPKα1 protein expression as compared to control values, while no change was observed in

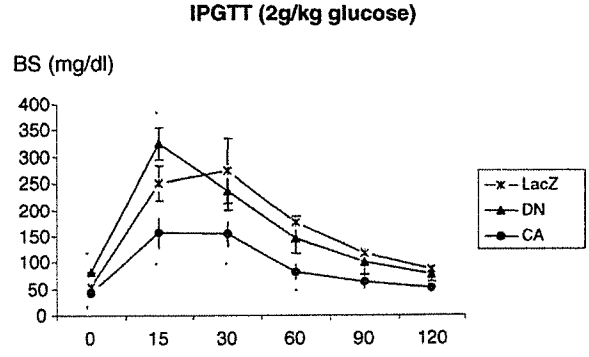

Fig. 2. Glucose tolerance testing of CAα1 and DNα1 mice. A significant difference in blood glucose levels is observed 15 min after glucose (2 g/kg) infusion ($^{*}P < 0.05$ vs. LacZ).

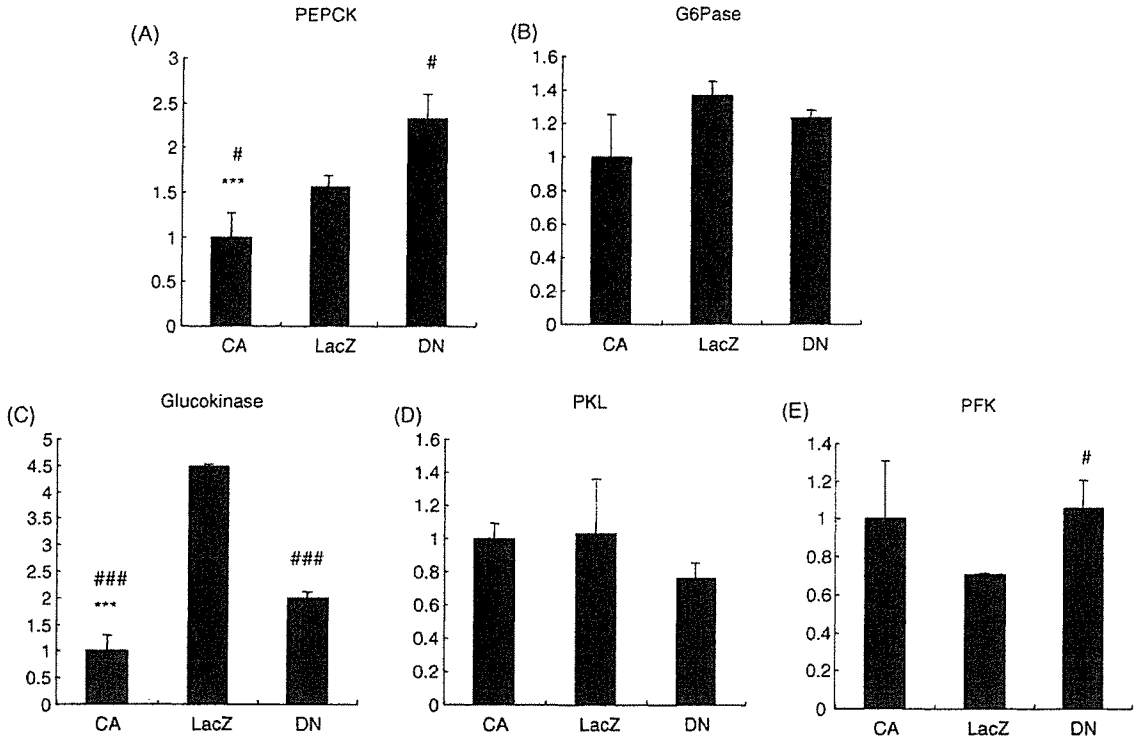

Fig. 3. The effects of constitutively active and dominant negative AMPKα1 on glucose metabolism. Total RNA was isolated and RNase protection assay was performed as described in Section 2. (A) Decreased mRNA of PEPCK, a key enzyme of gluconeogenesis, in CAα1 mice compared to that of LacZ and DNα1. (B) No change in G6Pase mRNA. (C) Decreased mRNA of glucokinase, a key enzyme of glycolysis, in CAα1 mice compared to that of LacZ and DNα1. (D and E) No significant change in either phosphofructokinase or on pyruvate kinase mRNA ($^{***}P < 0.05$ vs. DNα1, $^{\#}P < 0.05$ vs. LacZ and $^{\#\#\#}P < 0.001$ vs. LacZ).

AMPKα2 protein expression. Dexamethasone incubation also induced an increase in basal AMPK activity, by 50% and 100% for 12 and 24 h, respectively ($P < 0.05$ and $P < 0.001$). AMPK activity with AICAR (500 μM) incubation was also increased in dexamethasone treated hepatocytes (Fig. 4I). A similar enhancing effect of dexamethasone was observed using immunoblot analysis with phopho-AMPK-Thr172 antibody (Fig. 4J).

4. Discussion

Various stimuli including muscle contraction, hypoxia and biguanide reportedly activate the AMPK. In muscle, AMPK activation promotes Glut4 translocation from an internal pool to the cell surface increasing glucose transport [3]. In the liver, recent studies have found that AMPK activation by metformin [26], AICAR [21] or overexpression of the constitutively active form of AMPKα1 have marked effects on the expressions of a number of lipogenic enzymes [19]. In addition, the activation of AMPK by AICAR reportedly exerted strong effects on the activity and expression of glycolytic and gluconeogenic key enzymes, implying that AMPK activation may be involved in the regulation of gene transcription [11,22,23]. However, results obtained with AICAR stimulation must be interpreted with caution, as its effects are not restricted to AMPK activation [12]. Alternatively, it is possible to use adenovirus-mediated gene transfer to express these mutants in order to alter AMPK activity. Indeed, in a previous study in which CAα1 and DNα1 adenovirus overexpression systems were used for primary rat hepatocytes, it was suggested that glucose exerts regulatory effects on gene expressions by directly inhibiting AMPK [19].

The first aim of this study was to elucidate the role of AMPK activation in hepatic glucose homeostasis in vivo. For this purpose, we generated recombinant adenoviruses to express constitutively active (CAα1) [24] and dominant negative (DNα1) forms of the AMPKα1 subunit. These mutated AMPKα1 subunits were successfully overexpressed almost exclusively in the liver, and DNα1 mice were shown to be less glucose tolerant than the CAα1 mice, judging from the IPGTT (Fig. 2), with a higher fasting blood glucose concentration. From our data, it is not possible to clarify the exact

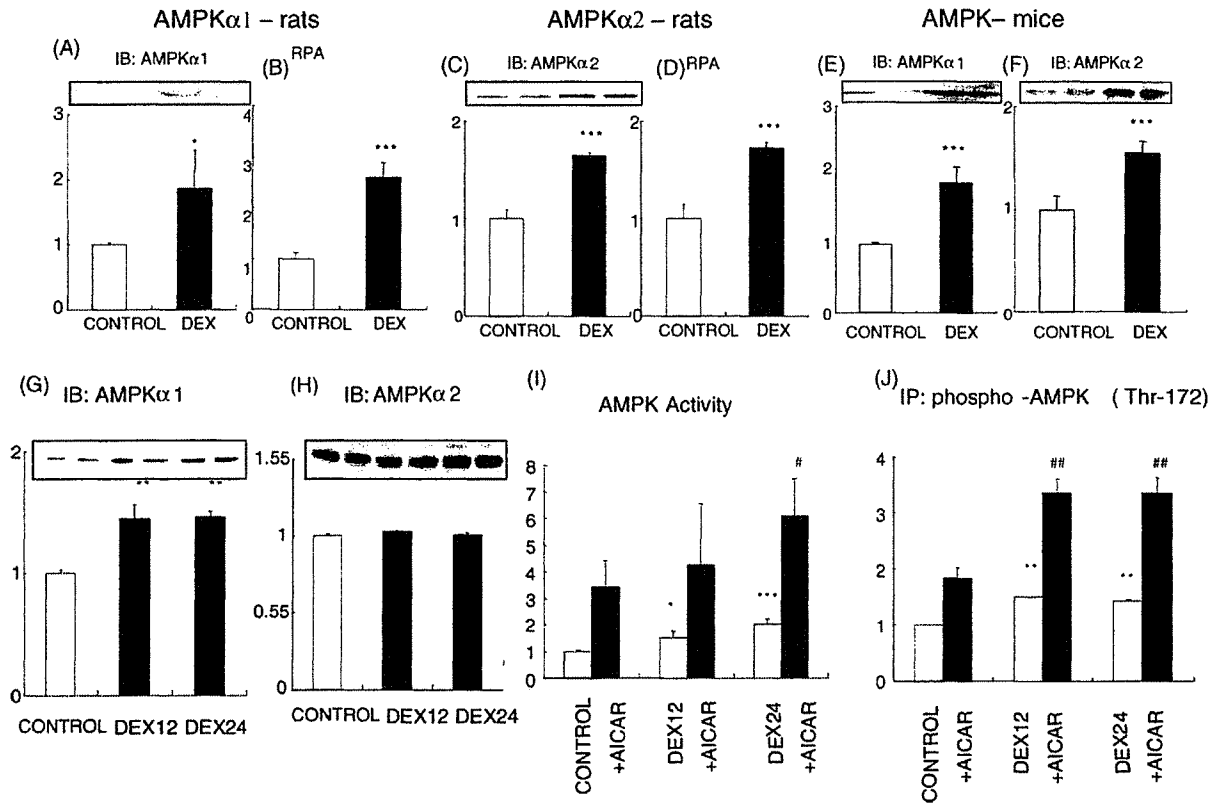

Fig. 4. Dexamethasone treatment increases AMPKα1 and α2 subunit protein contents and mRNA levels in rat and mice liver (A–F) and increases AMPKα1 protein expression, activity and phosphorylation in hepatocytes (G–J). (A) AMPKα1 protein expression in rats liver. IB with AMPKα1 subunit antibody. (B) AMPKα1 mRNA. Total RNA was isolated, and RNase protection assay was performed as described in Section 2. (C) AMPKα2 protein expression on rats liver. IB with AMPKα2 subunit antibody. (D) AMPKα2 mRNA. (E) AMPKα1 protein expression in mice liver. (F) AMPKα2 protein expression in mice liver. Cells were incubated in the absence or presence of dexamethasone (12 and 24 h). One hour later the medium was changed to KRBB, AICAR was added (500 mM). Cells were harvested after 1 h. (G) AMPKα1 protein expression. Cell lysates were immunoblotted (IB) with AMPKα1 subunit antibody ($^{**}P < 0.01$ vs. control). (H) AMPKα2 protein expression. IB with AMPKα2 subunit antibody. (I) AMPK activity. Lysates were immunopreciptated with AMPKα antibody and activity in the immunocomplexes was measured as a function of phosphorylation of SAMS peptide. (J) AMPK phosphorylation on threonine 172. Cell lysates were immunoblotted (IB) with phospho-AMPK (Thr172) antibody ($^{*}P < 0.05$ vs. control, $^{**}P < 0.01$ vs. control, $^{***}P < 0.001$ vs. control, $^{\#}P < 0.05$ vs. control + AICAR and $^{\#\#}P < 0.01$ vs. control + AICAR).

mechanisms underlying hyperglycemia after glucose load in DNα1 mice. However, we believe that the decrease in the gluconeogenic enzyme PEPCK (Fig. 3A) has a role on the decreased fasting glucose levels in CAα1 mice and we have some hypothesis to explain CAα1's IPGTT result.

In another study [25], it was shown that UCP-1, an AMPK activator, overexpression in liver not only exerts a remote beneficial effect on insulin sensitivity in muscle, by enhancement of muscular IRS-1 phosphorylation in response to insulin administration, but also is likely to convey signals, involving autonomic nerve network, to peripheral adipose tissues, promoting hydrolysis of triglycerides. This finding suggests that adenoviral mediated AMPK overexpression might also exert remote effects in muscle and liver metabolism.

In addition, in AMPKα2 knockout mice [26], decreased whole-body insulin sensitivity was suggested to be due to higher catecholamine urinary excretion in knockout mice than in controls. Since catecholamines are known to inhibit insulin release, deregulation in sympathetic tone could reduce insulin secretion, promoting glucose intolerance. Thus, an increase in sympathetic activation in DNα1 and concomitant glucose intolerance could also be considered.

Moreover, phosphorylation and inactivation of ACC, as a result of AMPK activation, serves to inhibit the proximal and rate limiting step of lipogenesis. Reduced synthesis of the ACC product, malonyl-CoA is also predicted to relieve inhibition of CPT-1, resulting in increased fatty acid oxidation. AMPK also mediates a decrease in SREBP-1 mRNA and protein expression,

which upregulation is postulated as a central mediator of insulin resistance, contributing to AMPK's effect in the modulation of circulating lipids and promotion of an increased liver insulin sensitivity [20]. In an opposite scenario, by DNα1 overexpression, an increase in plasma glucose and triglycerides could exert a decrease in muscle glucose transport by impairment of insulin sensitivity. Therefore, it could be possible that a remote effect of CAα1 and DNα1 overexpression might regulate whole-body insulin sensitivity and glucose uptake.

We also investigated the effects of dexamethasone on hepatic AMPK expression and its kinase activity using rats and primary cultured hepatocytes. AMPKα1 and α2 subunit protein expressions and mRNA levels were shown to be increased in the rat liver after 5 days of dexamethasone treatment. In addition, similarly, in primarily cultured mouse hepatocytes, α1 subunit protein expression and AMPK kinase activity were increased by dexamethasone treatment. Interestingly, this altered expression of AMPK by dexamethasone was not observed in muscle (data not shown). The upregulation in AMPK by dexamethasone was unexpected, since AMPK activation has been postulated to decrease hepatic glucose output and glucose-activated gene expression. To date, several molecular mechanisms have been reported to underlie dexamethasone-induced glucose intolerance, but the increased expression of AMPK described herein is a novel finding. Rather, such increased expression of AMPK can be regarded as a function compensating for the other glucose and lipid metabolic processes altered by dexamethasone. This report is thus the first to demonstrate the dexamethasone-induced regulation of AMPK expression.

Taken together, our observations suggest that the AMPK expression is an important factor in determining glucose tolerance and that this expression is affected by dexamethasone. Although further studies are necessary to elucidate the role of AMPK in the liver, we speculate that various hormones and growth factors alter hepatic glucose and lipid metabolic processes via altered AMPK expression.

References

[1] D.G. Hardie, I.P. Salt, S.A. Hawley, S.P. Davies, AMP-activated protein kinase: an ultrasensitive system for monitoring cellular energy charge, Biochem. J. 338 (1999) 717–722.

[2] S.A. Hawley, M.A. Selbert, E.G. Goldstein, A.M. Edelman, D. Carling, D.G. Hardie, 5′-AMP activates the AMP-activated protein kinase cascade, and Ca^{2+}/calmodium activates the calmodium-dependent protein kinase I cascade, via three independent mechanisms, J. Biol. Chem. 270 (1995) 27186–27191.

[3] T. Hayashi, M.F. Hirshman, E.J. Kurth, W.W. Winder, L.J. Goodyear, Evidence for 5′AMP-activated protein kinase mediation of the effect of muscle contraction on glucose transport, Diabetes 47 (1998) 1369–1373.

[4] A.H. Khan, J.E. Pessin, Insulin regulation of glucose uptake: a complex interplay of intracellular signaling pathways, Diabetologia 45 (2002) 1475–1483.

[5] J.E. Sullivan, K.J. Brocklehurst, A.E. Marley, F. Carey, D. Carling, R.K. Beri, Inhibition of lipolysis and lipogenesis in isolated rat adipocytes with AICAR, a cell permeable activator of AMP-activated protein kinase, FEBS Lett. 353 (1994) 33–36.

[6] D. Vavvas, A. Apazidis, A.K. Saha, et al., Contraction-induced changes in acetyl-CoA carboxylase and 5′AMP-activated kinase in skeletal muscle, J. Biol. Chem. 272 (1997) 13255–13261.

[7] R. Bergeron, R.R. Russel III, L.H. Young, et al., Effect of AMPK activation on muscle glucose metabolism in conscious rats, Am. J. Physiol. Endocrinol. Metab. 276 (1999) E938–E944.

[8] M.A. Iglesias, J.M. Ye, G. Frangioudakis, et al., AICAR administration causes an apparent enhancement of muscle and liver insulin action in insulin-resistant high-fat-fed rats, Diabetes 5188 (2002) 2886–2894.

[9] M. Foretz, D. Carling, C. Guichard, P. Ferre, F. Foufelle, AMP-activated protein kinase inhibits the glucose-activated expression of fatty acid synthase gene in rat hepatocytes, J. Biol. Chem. 272 (1998) 14767–14771.

[10] I. Leclerc, A. Kahn, B. Doiron, The AMP-activated protein kinase inhibits the transcriptional stimulation by glucose in liver cells, action through the glucose response complex, FEBS Lett. 431 (1998) 180–184.

[11] P.A. Lochhead, I.P. Salt, K.S. Walker, D.G. Hardie, C. Sutherland, 5-Aminoimidazole-4-carboxamide ribose mimics the effects of insulin on the expression of the 2 key gluconeogenic genes PEPCK and glucose-6-phosphatase, Diabetes 49 (2000) 896–903.

[12] H. Sakoda, T. Ogihara, M. Anai, et al., Activation of AMPK is essential for AICAR-induced glucose uptake by skeletal muscle but not adipocytes, Am. J. Physiol. Endocrinol. Metab. 282 (2002) E1239–E1244.

[13] L. Coderre, G.A. Vallega, P.F. Pilch, S.R. Chipkin, In vivo effects of dexamethasone and sucrose on glucose transport (GLUT-4) protein tissue distribution, Am. J. Physiol. 271 (1996) E643–E648.

[14] D. Argaud, Q. Zhang, W. Pan, S. Maitra, S.J. Pilkis, A.J. Lange, Regulation of rat liver glucose-6-phosphatase gene expression in different nutritional and hormonal states, Diabetes 45 (1996) 1563–1571.

[15] H. Sakoda, T. Ogihara, M. Anai, et al., No correlation of plasma cell 1 overexpression with insulin resistance in diabetic rats and 3T3-L1 adipocytes, Diabetes 48 (1999) 1365–1371.

[16] M.N. Berry, D.S. Friend, High-yield preparation of isolated rat liver parenchyma cells, J. Cell Biol. 43 (1969) 506–520.

[17] S.C. Stein, A. Woods, N.A. Jones, M.D. Davison, D. Carling, The regulation of AMP-activated protein kinase by phosphorylation, Biochem. J. 345 (2000) 437–443.

[18] C.C. Allain, L.S. Poon, C.S. Chan, W. Richmond, P.C. Fu, Enzymatic determination of total serum cholesterol, Clin. Chem. 20 (1974) 470–475.

[19] A. Woods, D. Azzout-Marniche, M. Foretz, et al., Characterization of the role of AMP-activated protein kinase in the regulation of glucose-activate gene expression using constitutively active and dominant negative forms of the kinase, Mol. Cell. Biol. 20 (2000) 6704–6711.

[20] G. Zhou, R. Myers, Y. Li, et al., Role of AMP-activated protein kinase in mechanism of metformin action, J. Clin. Invest. 108 (2001) 1167–1174.
[21] M. Zhou, B.Z. Lin, S. Coughlin, G. Vallega, P.F. Pilch, UCP-3 expression in skeletal muscle: effects of exercise, hypoxia, and AMP-activated protein kinase, Am. J. Physiol. Endocrinol. Metab. 279 (2000) E622–E629.
[22] J.F. Decaux, B. Antoine, A. Kahn, Regulation of expression of the L-type pyruvate kinase gene in adult rat hepatocytes in primary culture, J. Biol. Chem. 264 (1989) 11584–11590.
[23] A. Hubert, A. Husson, A. Chedeville, A. Lavoinne, AMP-activated protein kinase counteracted the inhibitory effect of glucose on the phosphoenolpyruvate carboxykinase gene expression in rat hepatocytes, FEBS Lett. 481 (2000) 209–212.
[24] B.E. Crute, K. Seefeld, J. Gamble, B.E. Kemp, L.A. Witters, Functional domains of the α1 catalytic subunit of the AMP-activated protein kinase, J. Biol. Chem. 273 (1998) 35347–35354.
[25] Y. Ishigaki, H. Katagiri, T. Yamada, et al., Dissipating excess energy stored in liver is a potential treatment strategy for diabetes associated with obesity, Diabetes 54 (2005) 322–332.
[26] B. Viollet, F. Andreelli, S.B. Jorgensen, et al., The AMP-activate protein kinase α2 catalytic subunit controls whole-body insulin sensitivity, J. Clin. Invest. 111 (2003) 91–98.

Available online at www.sciencedirect.com
SCIENCE DIRECT
Biochemical and Biophysical Research Communications 339 (2006) 533–539
BBRC
www.elsevier.com/locate/ybbrc

Transcriptional activity of Pax3 is co-activated by TAZ ☆

Masao Murakami [a,c,1], Junji Tominaga [a,b,1], Ryosuke Makita [b], Yasunobu Uchijima [b], Yukiko Kurihara [b], Osamu Nakagawa [c], Tomoichiro Asano [b], Hiroki Kurihara [b,*]

[a] *Department of Integrative Cell Biology, Institute of Molecular Embryology and Genetics, Kumamoto University, 2-2-1 Honjo, Kumamoto, Kumamoto 860-0811, Japan*
[b] *Department of Physiological Chemistry and Metabolism, Graduate School of Medicine, The University of Tokyo, 7-3-1 Hongo, Bunkyo-ku, Tokyo 113-0033, Japan*
[c] *Division of Cardiology, Department of Internal Medicine, and Department of Molecular Biology, The University of Texas Southwestern Medical Center at Dallas, 6000 Harry Hines Blvd., Dallas, TX 75390-9148, USA*

Received 11 October 2005
Available online 15 November 2005

Abstract

Pax3 is a transcription factor which functions in embryonic development and human diseases. In a yeast two-hybrid screen with full-length Pax3 as bait, we isolated a clone encoding transcriptional co-activator with PDZ-binding motif (TAZ) from an E10.5 mouse embryo cDNA library. Co-immunoprecipitation and nuclear co-localization of TAZ with Pax3 suggest that their association is functionally relevant. In situ hybridization revealed *TAZ* and *Pax3* expression to partially overlap in the paraxial mesoderm, limb buds, and the neural tube. In C2C12 myoblast cells and NIH3T3 cells, TAZ enhanced the transcriptional activity of Pax3 on artificial and microphthalmia-associated transcription factor promoter-luciferase constructs, suggesting that TAZ can function as a co-activator of Pax3. Functional interaction between Pax3 and TAZ may provide a clue to clarifying the mechanism by which Pax3 serves as a transcriptional activator during embryogenesis.

Keywords: Pax3; TAZ; Co-activator; Transcription

Pax3 is a member of the Pax gene family, consisting of nine members defined by a highly conserved DNA binding domain known as the paired domain (PD), which shares sequence homology with *Paired*, a *Drosophila* segmentation gene [1–3]. Pax3 also possesses a homeodomain (HD), another conserved DNA binding motif, and acts as a transcription factor to regulate the expression of genes, such as c-*ret*, c-*met*, and *MITF* [4–6]. During embryogenesis, Pax3 is expressed in the dorsal neural tube, neural crest derivatives, and paraxial mesoderm-derived skeletal muscle progenitors [1–3]. *Splotch* mice, harboring spontaneous mutations in *Pax3*, demonstrate defects in neural tube closure, cardiovascular morphogenesis, pigmentation, and limb myogenesis [7–10]. In humans, Waardenburg syndrome type I and III, characterized by facial, hearing, pigmentation, and limb abnormalities, are caused by mutations in *PAX3* [11–13]. Furthermore, PAX3-FKHR, a fusion protein between the C-terminal transactivation domain of FKHR (FOXO1A) and the DNA binding domain of Pax3 resulting from a chromosome translocation t (2; 13), can cause alveolar rhabdomyosarcomas [14–16].

To date, several nuclear proteins, such as Daxx and pRb, have been shown to interact physically with Pax3 and inhibit Pax3 activity [17,18]. HIRA, a homolog of the yeast transcriptional corepressors Hir1p and Hir2p, and Mox2, an Antennapedia-like homeobox-containing protein, have also been reported to associate with Pax3,

☆ *Abbreviations:* TAZ, transcriptional co-activator with PDZ-binding motif; YAP, yes-associated protein; MITF, microphthalmia-associated transcription factor; GST, glutathione *S*-transferase.

* Corresponding author. Fax: +81 3 5684 4958.
E-mail address: kuri-tky@umin.ac.jp (H. Kurihara).

[1] These authors contributed equally to this work.

0006-291X/$ - see front matter © 2005 Elsevier Inc. All rights reserved.
doi:10.1016/j.bbrc.2005.10.214

but their effects on the transcriptional activity of Pax3 have yet to be determined [19,20]. To obtain further information about protein–protein interactions modulating the function of Pax3, we screened for proteins that bind to Pax3 using the yeast two-hybrid system. Herein we identified TAZ as a molecule that binds to Pax3. We showed TAZ and Pax3 to be co-expressed in the paraxial mesoderm, limb buds and the neural tube during embryogenesis, and to be co-localized in the nucleus. Furthermore, TAZ can stimulate the transcriptional activity of Pax3 in cultured cells. These findings suggest that TAZ serves as a transcriptional co-activator for Pax3 and that this association may contribute to embryonic development.

Materials and methods

Plasmid constructions. Mouse Pax3 and TAZ cDNAs were amplified by PCR from E10.5 mouse embryo cDNA. Pax3 cDNA was subcloned into pDBLeu vector (Life Technologies) to generate pDBLeu-Pax3 as bait for the yeast two-hybrid screening. Pax3 or TAZ cDNAs were cloned into the 3′ cloning sites of the epitope-tagged expression vectors pCEFL-AU5 [21], pCEFL-HA [21], and pGEX (Amersham Pharmacia Biotech). Point mutants of Pax3 were constructed using a Quick Change XL Site-Directed Mutagenesis kit (Stratagene) and were inserted into the expression vectors. For p(PRS-1/-4)$_3$-Luc, a reporter construct for the luciferase assay, two oligonucleotides complementary to each other, 5′-ATTA CGTTCCAGATTACGTTCCAGATTACGTTCC-3′ and 5′-GGAACG TAATCTGGAACGTAATCTGGAACGTAAT-3′ were annealed and ligated to the minimal promoter in pLuc-MCS. For pMITF-Luc, the 5′-flanking sequence of the mouse *Mitf* gene (−387 to +99) was cloned by PCR from mouse genomic DNA and inserted into pGL3-Basic (Promega).

Yeast two-hybrid screening. Yeast two-hybrid screening was carried out according to the manufacturer's protocol for the ProQuest two-hybrid system (Life Technologies).

Cell culture and transfection. Cell culture conditions of 293T, NIH3T3, and C2C12 cells are described previously [22]. Transfection was performed using Lipofectamine Plus reagent (Life Technologies).

Pull-down assay, co-immunoprecipitation, and Western blotting. Preparation of GST-fusion proteins and cell lysates is described previously [22,23]. GST, GST-TAZ, and derivatives bound to glutathione beads were incubated at 4 °C for more than 2 h with cell lysates prepared from 293T cells expressing AU5-Pax3 proteins. After extensive washing, bound proteins were detected by Western blotting. For co-immunoprecipitation (co-IP) experiment, cell lysates of 293T cells expressing exogenous proteins were treated with anti-AU5 antibody and the immunoprecipitants were subjected to 10% SDS–PAGE. Proteins binding to AU5-Pax3 were detected by Western blotting using anti-HA antibody (Covance), as described previously [22,23].

In situ hybridization. Antisense and sense RNA probes were prepared from cDNA fragments by T3 or T7 RNA polymerase using a DIG RNA labeling kit (Roche). The procedure of in situ hybridization was described previously [24].

Preparation of anti-TAZ antibody. Polyclonal antibody against mouse TAZ was generated by injecting a rabbit with GST-TAZ. The bleeds were affinity-purified using Affi-Gel 10 gel (Bio-Rad) coupled with TAZ.

Immunocytochemistry. Cells were fixed with 4% paraformaldehyde in PBS, permeabilized with 0.2% Triton X-100 in PBS and washed with PBS at room temperature. After blocking with 5% skim milk in PBS, cells were incubated with the rabbit anti-TAZ antibody and mouse monoclonal anti-AU5 antibody. Then, cells were stained with secondary antibodies (FITC-conjugated donkey anti-rabbit IgG or rhodamine-conjugated goat anti-mouse IgG (Jackson Immunoresearch)) and viewed using a confocal microscope (Nikon D-ECLIPSE C1).

Luciferase assay. AU5- or HA-tagged expression constructs, reporter constructs, and pRL-SV40 (Promega) were co-transfected into C2C12 or NIH3T3 cells. Forty-eight hours after transfection, luciferase units in the cell lysates were determined with a luminometer. Transfection efficiency was normalized on the basis of *Renilla* luciferase activity.

Results

Identification of TAZ as a Pax3-binding protein

Using full-length Pax3 as bait, we screened about 2 million clones of the mouse E10.5 cDNA library for novel interacting partners. Thirty-four positive clones were obtained in the first screening, and the second screening with higher stringency revealed 6 clones to be candidates for Pax3-binding molecules. One was identified as encoding 359 amino acids (37–395) of TAZ, a transcriptional co-activator with PDZ-binding motif.

To demonstrate that Pax3 can physically interact with TAZ, we cloned full length TAZ and performed GST pull-down assay. As shown in Fig. 1A, Pax3 specifically associated with GST-TAZ but not with GST alone. To examine whether Pax3 can associate with TAZ in mammalian cells, we co-expressed AU5-Pax3 and HA-TAZ in 293T cells and performed co-IP experiments. HA-TAZ was coimmunoprecipitated only in the presence of Pax3 (Fig. 1B). These results indicate that Pax3 specifically interacts with TAZ both in vitro and in vivo.

Co-expression of TAZ and Pax3 in paraxial mesoderm, limb buds, and neural tube

Next, we investigated whether *TAZ* and *Pax3* genes are co-expressed in mouse embryonic tissues. In E9.5 embryos,

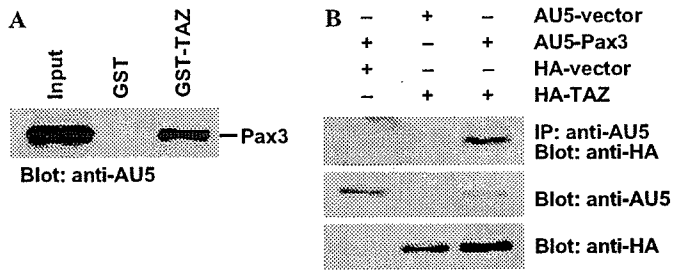

Fig. 1. Physical association between TAZ and Pax3. (A) Pull-down assay was performed using GST-TAZ, and AU5-Pax3 expressed in 293T cells. Interaction was detected by Western blotting using anti-AU5 antibody. (B) Co-IP experiment was performed using HA-TAZ and AU5-Pax3 expressed in 293T cells (upper). Expression of each protein was analyzed by Western blotting (lower).

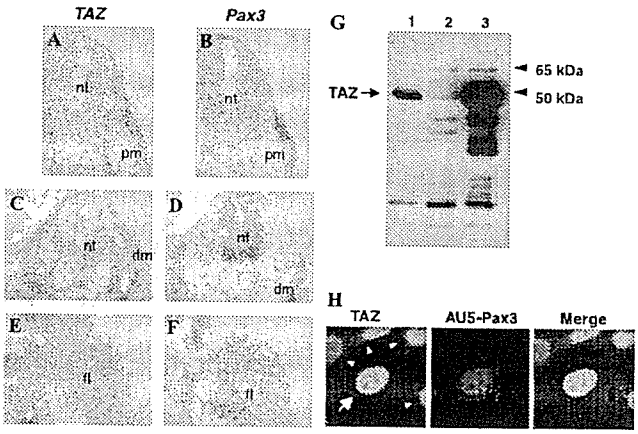

Fig. 2. Embryonic expression of TAZ and subcellular localization of TAZ in cultured cells. In situ hybridization with probes for *TAZ* (A,C,E) and *Pax3* (B,D,F) was performed on transverse sections of E9.5 (A,B) and E10.5 (C–F) mouse embryos. (A,B) Adjacent sections of an E9.5 embryo at the post-otic level. (C-F) Adjacent sections of an E10.5 embryo at the forelimb level. dm, dermomyotome; fl, forelimb; nt, neural tube; pm, paraxial mesoderm. (G) Western blot of endogenous and overexpressed TAZ: NIH3T3 (lane 1), 293T (lane 2), and AU5-TAZ-transfected 293T cells (lane 3). (H) Immunocytochemistry of NIH3T3 cells transfected with AU5-Pax3. Arrow and arrowheads indicates a Pax3-transfected cell and untransfected cells, respectively.

TAZ expression was detected in the paraxial mesoderm (Fig. 2A), where it partially overlapped with *Pax3* expression in dermomyotomes (Fig. 2B and [25,26]). In E10.5 embryos, *TAZ* expression was distributed in the somitic mesoderm and limb bud mesenchyme (Figs. 2C and E). At the same stage, *Pax3* was expressed in dermomyotomes and migrating muscle progenitors in limb buds (Figs. 2D and F and [25,26]). Thus, *TAZ* was co-expressed with *Pax3* in the skeletal muscle cell lineage, but appeared to be more diffuse than *Pax3* expression, suggesting *TAZ* to be widely expressed beyond the muscle cell lineage within the mesoderm.

TAZ was also expressed in the ventral and medial part of the neural tube at E10.5 (Fig. 2C). In contrast, *Pax3* was expressed in the dorsal half of the neural tube (Fig. 2D). Comparison of the expression domains of both genes indicates that *TAZ* and *Pax3* are co-expressed in the intermediate region between the dorsoventral halves (Figs. 2C and D).

Nuclear localization of TAZ in cultured cells

Next, we generated a rabbit polyclonal antibody against mouse TAZ and analyzed endogenous TAZ protein. Western blot analysis of lysates from NIH3T3 cells revealed this antibody to recognize a single band with a molecular mass of approximately 50 kDa (Fig. 2G, lane 1), which corresponded to the most intense band in 293T cells transfected with TAZ (Fig. 2G, lane 3).

We analyzed subcellular localization of TAZ and Pax3 in NIH3T3 cells. Endogenous TAZ immunoreactivity was detected predominantly in the nucleus, where exogenous Pax3 was also localized (Fig. 2H). TAZ was localized in the cytoplasm as well, but to a lesser extent (Fig. 2H). This result indicates that TAZ may act as a nuclear protein and interact with Pax3 in the nucleus.

TAZ acts as a transcriptional co-activator for Pax3

It is reported that TAZ can function as a co-activator of transcription factors [27–30]. To test whether TAZ can co-activate Pax3-dependent transcription, we performed a luciferase assay using the reporter plasmid in which three copies of the Pax3 binding element for both the HD and the PD (ATTA and GTTCC, respectively) were placed upstream from the luciferase gene (p(PRS-1/-4)$_3$-Luc) [9]. In C2C12 cells, Pax3 produced a 6-fold increase in luciferase activity as compared with the control (Fig. 3A). Co-expression of TAZ further augmented Pax3-dependent transcription in a dose-dependent manner (Fig. 3A). TAZ alone increased the basal transcription level by ~3.5-fold (Fig. 3A), possibly due to the presence of Pax3 or related transcription factors in C2C12 cells. We then examined the effect of TAZ on basal and Pax3-activated transcription in NIH3T3 cells, in which TAZ was expressed but Pax3 was not. Pax3 enhanced transcriptional activity by ~5.8-fold, and co-transfection of TAZ with Pax3 resulted in a ~11-fold increase in transcriptional activity over basal levels (Fig. 3B). However, transfection of TAZ alone did not enhance the basal activity at all (Fig. 3B).

To further confirm the co-activation of Pax3 by TAZ, we used pMITF-Luc, a reporter plasmid containing the promoter region of mouse *Mitf* gene. Pax3 or TAZ alone increased luciferase activity by ~7.7- and 2.2-fold as compared with the control, respectively (Fig. 3C). Co-transfection of TAZ with Pax3 resulted in a ~17-fold increase in luciferase activity (Fig. 3C). This result is consistent with the possibility that TAZ may act as a transcriptional co-activator of Pax3.

TAZ interacted with Pax3 via multiple domains

To identify the interaction domain, we made deletion mutants of Pax3 and TAZ as shown in Fig. 4 and examined their interactions by GST pull-down assay. Pax3 interacted with both TAZ (1–170) and TAZ (171–395) (Fig. 5A). TAZ also interacted with both Pax3-NM and Pax3-C (Fig. 5B). These results suggest that the interaction between Pax3 and TAZ may be through multiple domains. Pax3 has two L/PPXY motifs (PY-motifs) in its C-terminal region (Fig. 4). We have introduced point mutations into these sites to analyze the importance of the PY-motifs for interaction with TAZ. As shown in Fig. 5C, Pax3-C interacts with TAZ, but not Pax3C-AY, -YA, and -AA, suggesting that the interaction between C-terminal region of Pax3 and TAZ are through WW domain and PY-motif. To analyze which interactions are the strongest and the most specific, we made additional deletion mutants of TAZ and examined Pax3–TAZ interactions using more stringent

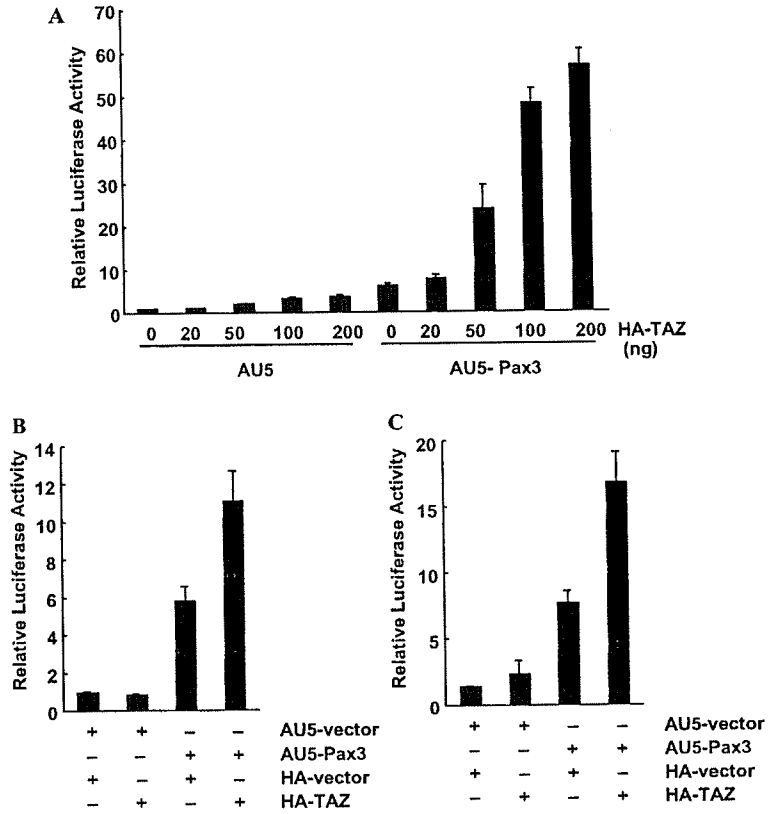

Fig. 3. TAZ coactivated Pax3-dependent transcription. (A) TAZ activated Pax3-dependent transcription in a dose-dependent manner. Different amounts of TAZ expression vector were cotransfected with 100 ng Pax3 vector and p(PRS-1/-4)$_3$-Luc into C2C12 cells, and luciferase assay was performed. (B) Luciferase assay was performed using NIH3T3 cells not expressing Pax3. (C) *MITF*-Luc was cotransfected together with expression vectors for TAZ (100 ng) and Pax3 (100 ng) into C2C12 cells, and luciferase assay was performed. Each value is expressed as the mean ± standard deviation of triplicate experiments.

conditions. As shown in Fig. 5D, a small fragment of TAZ (100–170) containing the WW domain physically interacted with both full length Pax3 and Pax3-C but not with Pax3-N or Pax3-M. To confirm the interaction of TAZ-WW domain is specific to PY-motif, we performed pull-down assay using Pax3 mutant lacking the PY-motifs. As shown in Fig. 5E, Pax3 but not Pax3-AA can bind to the TAZ-WW domain, indicating the interaction between TAZ-WW domain and Pax3 is PY-motif-specific. Under these conditions, TAZ (171–395) did not bind to Pax3 (Fig. 5D), suggesting a hypertonic condition might affect the interaction between the C-terminal region of TAZ and Pax3.

PY-motifs of Pax3 are not essential for the co-activation by TAZ

Next, we tested whether the association between the (L/P)PXY motif of Pax3 and the WW domain of TAZ was necessary for transcriptional co-activation by TAZ. For this purpose, we performed a reporter assay using point mutants of Pax3 lacking either or both of the two (L/P)PXY motifs. All the mutants tested, Pax3-AY, Pax3-YA, and Pax3-AA, activated transcription to the same degree as wild-type Pax3 (Fig. 6A). As shown in Fig. 6B, these Pax3 mutants without PY-motifs as well as wild-type Pax3 interacted with TAZ, suggesting that an interaction other than between the WW domain and PY-motifs is also important for the interaction with TAZ. Instead, Pax3-NM (1–285), a mutant lacking the C-terminal region, demonstrated neither transcriptional activation nor co-activation by TAZ (Fig. 6A). These results suggest that the C-terminal region of Pax3 may be essential for co-activation by TAZ, while the (L/P)PXY motifs in this region are not required and another interaction may be more important in vivo.

Discussion

In this study, we identified TAZ as a co-activator of Pax3. TAZ physically interacted with Pax3 and co-activated Pax3-dependent transcription on artificial and *Mitf* promoter-luciferase constructs.

Although Pax3 influences the expression of various genes during embryonic development, its mode of action

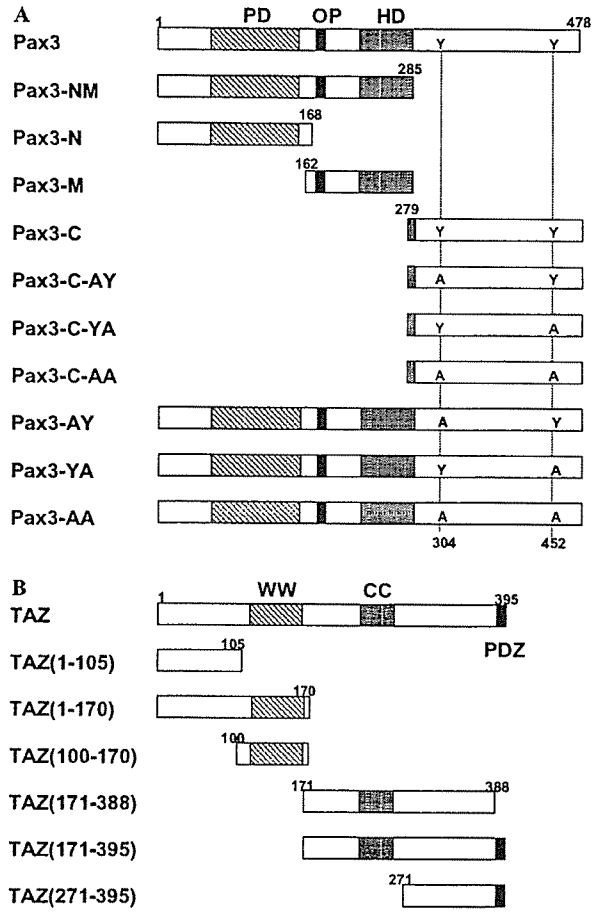

Fig. 4. The structures of mouse Pax3, TAZ, and mutated derivatives used in this study. (A) Pax3 and its mutants. Tyrosines at positions 304 and 452 are substituted with alanines in some mutants. PD, paired domain; OP, octapeptide domain; HD, homeodomain. (B) TAZ and its deletion mutants. WW, WW domain; CC, coiled-coil domain; PDZ, PDZ-binding motif.

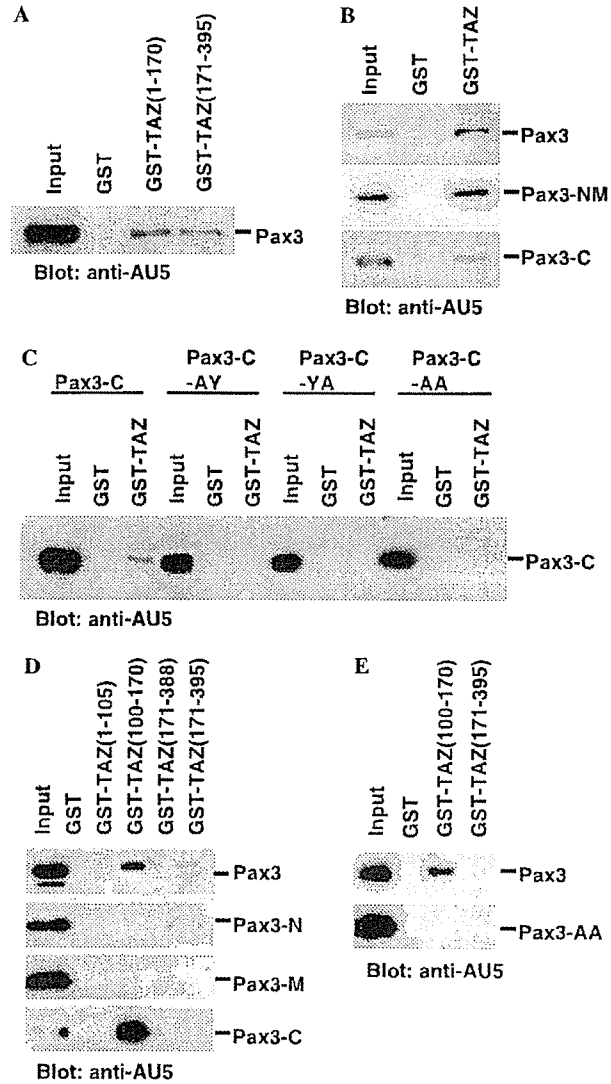

Fig. 5. Interaction domain analysis of TAZ and Pax3. (A–C) Pull-down assay was performed using GST-TAZ deletion mutants and AU5-Pax3 expressed in 293T cells. Bound proteins were detected by Western blotting using anti-AU5 antibody. (D,E) Pull-down assay using GST-TAZ deletion mutants and Pax3 mutants expressed in 293T cells in the presence of 0.5 M NaCl.

as a transcription factor remains poorly understood. Recently it has been reported that PAX3-FKHR, which is a potent gain-of-function mutation, rescues the defects of Pax3 mutant mice [14]. This suggests that Pax3 acts mainly as a transcriptional activator in vivo and indicates the importance of co-activators for Pax3 mediated transcription [14]. However, only co-repressors, such as Daxx and Rb [17,18], have been identified as Pax3 binding proteins to date. Our finding may be an important clue to elucidating the mechanisms that regulate Pax3 activity. Detailed analyses of TAZ may help to elucidate the activation mechanisms of Pax3.

TAZ was originally identified as a 14-3-3-binding molecule, and phosphorylation of TAZ affected the interaction with 14-3-3 and its subcellular localization [27]. This result suggests that the regulation of transcriptional activity by TAZ may be signal-responsive. TAZ shares homology with Yes-associated protein (YAP) especially in the WW domain, which is suggested to be responsible for binding to the (L/P)PXY motif present on interacting proteins. TAZ and YAP are expressed relatively ubiquitously [27] and might have the redundant function to co-activate the same transcription factors in some tissues.

Recently, it has been reported that TAZ acts as a transcriptional co-activator for Cbfa1, TTF1/Nkx2.1, and Runx2 [28–30]. Binding between the WW domain and (L/P)PXY motifs is assumed to mediate the interactions between TAZ and these transcriptional factors. Pax3 has two (L/P)PXY motifs in its C-terminal region. However, the present results indicate that TAZ can associate with Pax3 and co-activate its transcriptional activity without interaction between the WW domain and (L/P)PXY

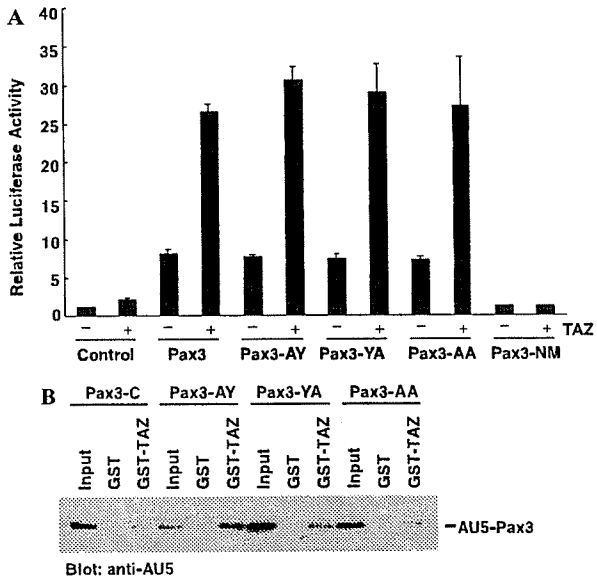

Fig. 6. (A) Expression vector for Pax3 mutants and TAZ were cotransfected with p(PRS-1/-4)$_3$-Luc into C2C12 cells, and luciferase assay was performed. Each value is expressed as the mean ± standard deviation of triplicate experiments. (B) Pull-down assay was performed using GST-TAZ and AU5-Pax3 mutants expressed in 293T cells. Bound proteins were detected by Western blotting using anti-AU5 antibody.

motifs. Deletion mutant analyses indicate either the N-terminal or C-terminal region of TAZ is sufficient for binding to Pax3 in pull-down assays, suggesting that TAZ binds to Pax3 via multiple domains. These results may suggest the possibility that TAZ can interact with transcription factors having no PY-motif and co-activate them. For Pax3 however, deletion of the C-terminal region abolished the basal and TAZ-dependent co-activation of transcription. This suggests that the C-terminal region of Pax3 is required for stimulation of gene expression, although the N-terminal region of Pax3 is sufficient for binding to TAZ in vitro. More detail analyses are necessary, and identification of other binding partners of TAZ may help us to elucidate the co-activation mechanisms of TAZ.

The present in situ hybridization analysis revealed *TAZ* and Pax3 expression to partially overlap in the paraxial mesoderm, limb buds, and the neural tube during mouse embryogenesis. This raises the possibility that TAZ and Pax3 may interact in a subset of myogenic and neurogenic cell lineages to regulate tissue-specific gene expression. However, the expression patterns of these two genes are markedly different overall, suggesting that the presence of TAZ may determine target gene specificity of Pax3. In non-myogenic cell lineages within the mesoderm, TAZ may associate with different transcription factors to control cell growth and differentiation.

In conclusion, TAZ has now emerged as a transcriptional co-activator for Pax3. This finding may provide an important clue to the mechanism by which the transcriptional activity of Pax3 is regulated and activates downstream genes to contribute to embryogenesis.

Acknowledgments

We thank Dr. E.M. Small for critical comments on this paper, and Ms. S. Okamura, Mr. Y. Kawamura, and Ms. K. Shin-Fukuhara for technical assistance. We are also grateful to members of the Gene Technology Center in Kumamoto University for their important contributions to the experiments. This work was supported by grants from the Japan Society for the Promotion of Science Research for the Future Program; Grants-in-Aid for scientific research from the Ministry of Education, Culture, Sports, Science and Technology, Japan; a Research Grant for Cardiovascular Diseases (14C-1) from the Ministry of Health, Labor and Welfare; a Research Grant from Uehara Memorial Foundation.

References

[1] M.D. Goulding, G. Chalepakis, U. Deutsch, J.R. Erselius, P. Gruss, Pax-3, a novel murine DNA binding protein expressed during early neurogenesis, EMBO J. 10 (1991) 1135–1147.
[2] A. Mansouri, M. Hallonet, P. Gruss, Pax genes and their roles in cell differentiation and development, Curr. Opin. Cell Biol. 8 (1996) 851–857.
[3] N. Chi, J.A. Epstein, Getting your Pax straight: Pax proteins in development and disease, Trends Genet. 18 (2002) 41–47.
[4] D. Lang, J.A. Epstein, Sox10 and Pax3 physically interact to mediate activation of a conserved c-RET enhancer, Hum. Mol. Genet. 12 (2003) 937–945.
[5] J.A. Epstein, D.N. Shapiro, J. Cheng, P.Y. Lam, R.L. Maas, Pax3 modulates expression of the c-Met receptor during limb muscle development, Proc. Natl. Acad. Sci. USA 93 (1996) 4213–4218.
[6] A. Watanabe, K. Takeda, B. Ploplis, M. Tachibana, Epistatic relationship between Waardenburg syndrome genes MITF and PAX3, Nat. Genet. 18 (1998) 283–286.
[7] D.J. Epstein, M. Vekemans, P. Gros, Splotch (Sp2H), a mutation affecting development of the mouse neural tube, shows a deletion within the paired homeodomain of Pax-3, Cell 67 (1991) 767–774.
[8] D.J. Epstein, K.J. Vogan, D.G. Trasler, P. Gros, A mutation within intron 3 of the Pax-3 gene produces aberrantly spliced mRNA transcripts in the splotch (Sp) mouse mutant, Proc. Natl. Acad. Sci. USA 90 (1993) 532–536.
[9] G. Chalepakis, M. Goulding, A. Read, T. Strachan, P. Gruss, Molecular basis of splotch and Waardenburg Pax-3 mutations, Proc. Natl. Acad. Sci. USA 91 (1994) 3685–3689.
[10] S.J. Conway, D.J. Henderson, A.J. Copp, Pax3 is required for cardiac neural crest migration in the mouse: evidence from the splotch (Sp2H) mutant, Development 124 (1997) 505–514.
[11] M. Tassabehji, A.P. Read, V.E. Newton, R. Harris, R. Balling, P. Gruss, T. Strachan, Waardenburg's syndrome patients have mutations in the human homologue of the Pax-3 paired box gene, Nature 355 (1992) 635–636.
[12] C.T. Baldwin, C.F. Hoth, J.A. Amos, E.O. da-Silva, A. Milunsky, An exonic mutation in the HuP2 paired domain gene causes Waardenburg's syndrome, Nature 355 (1992) 637–638.
[13] M. Tassabehji, A.P. Read, V.E. Newton, M. Patton, P. Gruss, R. Harris, T. Strachan, Mutations in the PAX3 gene causing Waardenburg syndrome type 1 and type 2, Nat. Genet. 3 (1993) 26–30.
[14] F. Relaix, M. Polimeni, D. Rocancourt, C. Ponzetto, B.W. Schafer, M. Buckingham, The transcriptional activator PAX3-FKHR rescues the defects of Pax3 mutant mice but induces a myogenic gain-of-function phenotype with ligand-independent activation of Met signaling in vivo, Genes Dev. 17 (2003) 2950–2965.

[15] F.G. Barr, N. Galili, J. Holick, J.A. Biegel, G. Rovera, B.S. Emanuel, Rearrangement of the PAX3 paired box gene in the paediatric solid tumour alveolar rhabdomyosarcoma, Nat. Genet. 3 (1993) 113–117.
[16] N. Galili, R.J. Davis, W.J. Fredericks, S. Mukhopadhyay, F.J. Rauscher 3rd, B.S. Emanuel, G. Rovera, F.G. Barr, Fusion of a fork head domain gene to PAX3 in the solid tumour alveolar rhabdomyosarcoma, Nat. Genet. 5 (1993) 230–235.
[17] A.D. Hollenbach, J.E. Sublett, C.J. McPherson, G. Grosveld, The Pax3-FKHR oncoprotein is unresponsive to the Pax3-associated repressor hDaxx, EMBO J. 18 (1999) 3702–3711.
[18] O. Wiggan, A. Taniguchi-Sidle, P.A. Hamel, Interaction of the pRB-family proteins with factors containing paired-like homeodomains, Oncogene 16 (1998) 227–236.
[19] P. Magnaghi, C. Roberts, S. Lorain, M. Lipinski, P.J. Scambler, HIRA, a mammalian homologue of Saccharomyces cerevisiae transcriptional co-repressors, interacts with Pax3, Nat. Genet. 20 (1998) 74–77.
[20] D. Stamataki, M. Kastrinaki, B.S. Mankoo, V. Pachnis, D. Karagogeos, Homeodomain proteins Mox1 and Mox2 associate with Pax1 and Pax3 transcription factors, FEBS Lett. 499 (2001) 274–278.
[21] C. Murga, L. Laguinge, R. Wetzker, A. Cuadrado, J.S. Gutkind, Activation of Akt/protein kinase B by G protein-coupled receptors. A role for α and $\beta\gamma$ subunits of heterotrimeric G proteins acting through phosphatidylinositol-3-OH kinase γ, J. Biol. Chem. 273 (1998) 19080–19085.
[22] M. Murakami, K. Kataoka, S. Fukuhara, O. Nakagawa, H. Kurihara, Akt-dependent phosphorylation negatively regulates the transcriptional activity of dHAND by inhibiting the DNA binding activity, Eur. J. Biochem. 271 (2004) 3330–3339.
[23] M. Murakami, K. Kataoka, J. Tominaga, O. Nakagawa, H. Kurihara, Differential cooperation dHAND and three distinct E-proteins, Biochem. Biophys. Res. Commun. 323 (2004) 167–174.
[24] Y. Yamaguchi, T. Nagase, R. Makita, S. Fukuhara, T. Tomita, T. Tominaga, H. Kurihara, Y. Ouchi, Identification of multiple novel epididymis-specific beta-defencin isoforms in humans and mice, J. Immunol. 169 (2002) 2516–2523.
[25] E. Bober, T. Franz, H.H. Arnold, P. Gruss, P. Tremblay, Pax-3 is required for the development of limb muscles: a possible role for the migration of dermomyotomal muscle progenitor cells, Development 120 (1994) 603–612.
[26] M. Goulding, A. Lumsden, A.J. Paquette, Regulation of Pax-3 expression in the dermomyotome and its role in muscle development, Development 120 (1994) 957–971.
[27] F. Kanai, P.A. Marignani, D. Sarbassova, R. Yagi, R.A. Hall, M. Donowitz, A. Hisaminato, T. Fujiwara, Y. Ito, L.C. Cantley, M.B. Yaffe, TAZ: a novel transcriptional co-activator regulated by interactions with 14-3-3 and PDZ domain proteins, EMBO J. 19 (2000) 6778–6791.
[28] C.B. Cui, L.F. Cooper, X. Yang, G. Karsenty, I. Aukhil, Transcriptional coactivation of bone-specific transcription factor Cbfa1 by TAZ, Mol. Cell Biol. 23 (2003) 1004–1013.
[29] K.S. Park, J.A. Whitsett, T. Di Palma, J.H. Hong, M.B. Yaffe, M. Zannini, TAZ interacts with TTF-1 and regulates expression of surfactant protein-C, J. Biol. Chem. 279 (2004) 17384–17390.
[30] J.H. Hong, E.S. Hwang, M.T. McManus, A. Amsterdam, Y. Tian, R. Kalmukova, E. Mueller, T. Benjamin, B.M. Spiegelman, P.A. Sharp, N. Hopkins, M.B. Yaffe, TAZ, a transcriptional modulator of mesenchymal stem cell differentiation, Science 309 (2005) 1074–1078.

Original Article

Involvement of Apolipoprotein E in Excess Fat Accumulation and Insulin Resistance

Junhong Gao,[1,2] Hideki Katagiri,[2] Yasushi Ishigaki,[1] Tetsuya Yamada,[1] Takehide Ogihara,[2] Junta Imai,[1,2] Kenji Uno,[1,2] Yutaka Hasegawa,[1,2] Makoto Kanzaki,[3] Tokuo T. Yamamoto,[4] Shun Ishibashi,[5] and Yoshitomo Oka[1]

Although apolipoprotein E (apoE) is well known to play a major role in lipid metabolism, its role in glucose and energy homeostasis remains unclear. Herein, we established apoE-deficient genetically obese Ay (apoE$^{-/-}$;Ay/+) mice. ApoE deficiency in Ay mice prevented the development of obesity, with decreased fat accumulation in the liver and adipose tissues. ApoE$^{-/-}$;Ay/+ mice exhibited better glucose tolerance than apoE$^{+/+}$;Ay/+ mice. Insulin tolerance testing and hyperinsulinemic-euglycemic clamp study revealed marked improvement of insulin sensitivity, despite increased plasma free fatty acid levels. These metabolic phenotypes were reversed by adenoviral replenishment of apoE protein, indicating circulating apoE to be involved in increased adiposity and obesity-related metabolic disorders. Uptake of apoE-lacking VLDL into the liver and adipocytes was markedly inhibited, but adipocytes in apoE$^{-/-}$;Ay/+ mice exhibited normal differentiation, suggesting that apoE-dependent VLDL transport is involved in the development of obesity, i.e., surplus fat accumulation. Interestingly, apoE$^{-/-}$;Ay/+ mice exhibited decreased food intake and increased energy expenditure. Pair-feeding experiments indicate these phenomena to both contribute to the obesity-resistant phenotypes associated with apoE deficiency. Thus, apoE is involved in maintaining energy homeostasis. ApoE-dependent excess fat accumulation is a promising therapeutic target for the metabolic syndrome. ***Diabetes*** **56:24–33, 2007**

From the [1]Division of Molecular Metabolism and Diabetes, Tohoku University Graduate School of Medicine, Sendai, Japan; the [2]Division of Advanced Therapeutics for Metabolic Diseases, Center for Translational and Advanced Animal Research, Tohoku University Graduate School of Medicine, Sendai, Japan; the [3]Tohoku University Bio-Engineering Research Organization, Sendai, Japan; the [4]Center for Advanced Genome Research, Institute of Development, Aging and Cancer, Tohoku University, Sendai, Japan; and the [5]Division of Endocrinology and Metabolism, Department of Medicine, Jichi Medical School, Tochigi, Japan.

Address correspondence and reprint requests to Hideki Katagiri, MD, PhD, Division of Advanced Therapeutics for Metabolic Diseases, Center for Translational and Advanced Animal Research, Tohoku University Graduate School of Medicine, 2-1 Seiryo-machi, Aoba-ku, Sendai 980-8575, Japan. E-mail: katagiri@mail.tains.tohoku.ac.jp.

Received for publication 1 February 2006 and accepted in revised form 16 October 2006.

J.G., H.K., and Y.I. contributed equally to this work.

Additional information for this article can be found in an online appendix at http://diabetes.diabetesjournals.org.

ApoE, apolipoprotein E; FFA, free fatty acid; HPLC, high-performance liquid chromatography; IRS, insulin receptor substrate; TNF, tumor necrosis factor; VLDLR, VLDL receptor.

DOI: 10.2337/db06-0144

Obesity causes various metabolic disorders, including diabetes, dyslipidemia, and hypertension and has become a major public health concern in most industrialized countries in recent decades (1). Obesity results mainly from excess energy intake and physical inactivity, and the molecular mechanisms of body weight control have been intensively studied from various aspects, including appetite, energy expenditure, glucose and lipid metabolism, and adiposity (2). Excess fat accumulation is associated with metabolic disorders including insulin resistance, glucose intolerance, and dyslipidemia (3). In addition, we reported that dissipating excess energy improves diabetes and obesity in mice (4). On the other hand, lipoatrophy also leads to these metabolic disorders in mice and humans. Fat-less mice (5,6) as well as patients with lipodystrophy (7) exhibit severe insulin resistance and diabetes. Thus, having an appropriate adipose tissue amount is important for maintaining glucose homeostasis via adipocyte metabolic activities including production and secretion of adipocytokines.

Apolipoprotein E (apoE) is a structural component of all lipoprotein particles except LDL and serves as a high-affinity ligand for lipoprotein receptors (8). ApoE plays important roles in hepatic uptake of chylomicron and VLDL remnants (9,10) as well as hepatic secretion of VLDL (11). In contrast, involvement of apoE in adiposity, insulin sensitivity, and glucose metabolism is somewhat controversial. ApoE$^{-/-}$ mice treated with gold thioglucose become obese and diabetic (12). High-fat chow induces obesity in apoE$^{-/-}$ mice in a manner similar to that in wild-type C57BL/6 mice, while apoE deficiency produced resistance to some obesity-related phenotypic features, including hyperinsulinemia and hyperglycemia (13). On the other hand, Chiba et al. reported that apoE deficiency in *ob/ob* mice resulted in neither increased body weight nor adiposity, but glucose metabolism and insulin sensitivity were not examined (14). They attributed decreased adiposity in *ob/ob*;apoE$^{-/-}$ mice to impaired adipocyte differentiation based on in vitro findings obtained using bone marrow stromal cells and 3T3-L1 cells. However, impaired adipocyte differentiation induces severe insulin resistance and diabetes (5,6), markedly different from the metabolic phenotypes of apoE$^{-/-}$ mice. Thus, it remains unclear how, and even whether, apoE is involved in adiposity and glucose metabolism.

Herein, we recognized that adult apoE$^{-/-}$ mice are leaner and more glucose tolerant than wild-type mice. In contrast, younger apoE$^{-/-}$ mice exhibit normal adiposity,

i.e., they are not lipoatrophic. These findings led us to postulate that apoE is involved in surplus fat accumulation, resulting in the development of insulin resistance, but does not play a major role in the fat accumulation required for adipocyte function. To clarify whether apoE is involved in the development of insulin resistance associated with obesity and, if so, to identify the underlying mechanisms, we established apoE-deficient genetically obese Ay ($apoE^{-/-}$;Ay/+) mice. Without impairing adipocyte differentiation in vivo, apoE deficiency in Ay mice prevented obesity, glucose intolerance, and insulin resistance. Interestingly, $apoE^{-/-}$;Ay/+ mice exhibited decreased food intake and increased energy expenditure, both of which contribute to the obesity-resistant phenotypes associated with apoE deficiency. Thus, apoE is a key molecule for development of obesity, i.e., excess fat accumulation, and is a possible therapeutic target for the metabolic syndrome.

RESEARCH DESIGN AND METHODS

Animal studies were conducted in accordance with the institutional guidelines for animal experiments at Tohoku University. $ApoE^{+/-}$;Ay/+ mice were obtained by mating male KKAy mice (Nippon CLEA, Shizuoka, Japan) and female apoE-deficient mice with the C57BL/6J background (15) (The Jackson Laboratory, Bar Harbor, ME). Male $apoE^{+/-}$;Ay/+ mice were mated with female $apoE^{+/-}$ mice with the C57BL/6J background. Mice of three genotyopes, $apoE^{+/+}$;Ay/+, $apoE^{+/-}$;Ay/+, and $apoE^{-/-}$;Ay/+, were selected. Littermates were used in each experiment. These mice were housed individually and started on a high-fat diet consisting of 15.3% (wt/wt) fat (Quick Fat; Nippon CLEA, Shizuoka, Japan) at 6 weeks of age. Experiments were performed 5 weeks after high-fat loading. Viruses were administered intravenously at a dose of 2×10^8 plaque-forming units 4 weeks after high-fat loading. For pair-feeding experiments, $apoE^{+/+}$;Ay/+ mice were allotted into two groups at 4 weeks of age. One group was given their daily food allotments based on the previous days' consumption by $apoE^{-/-}$;Ay/+ littermate mice.

Recombinant adenovirus preparation. Recombinant adenovirus, containing the human apoE2, E3, E4, or bacterial β-galactosidase gene (*Adex1CAlacZ*) cDNA under the CAG promoter, was prepared as described previously (16).

Oxygen consumption. Oxygen consumption was measured with an O_2/CO_2 metabolism measuring system (model MK-5000RQ; Muromachikikai, Tokyo, Japan) as described previously (4).

Histological analysis. Livers and adipose tissues were removed, fixed with 10% formalin, and embedded in paraffin. Tissue sections were stained with hematoxylin-eosin or 0.1% (wt/vol) Oil Red O. Total adipocyte areas were traced manually and analyzed. Brown and white adipocyte areas were measured in 100 or more cells per mouse in each group.

Triglyceride contents of the liver and adipose tissue. Frozen livers or adipose tissues were homogenized, and triglycerides were extracted with $CHCl_3$:CH_3OH (2:1 vol:vol), dried, and resuspended in 2-propanol. Triglyceride contents were measured using Lipidos liquid (Toyobo, Osaka, Japan).

Tyrosine phosphorylation of insulin receptor substrate 1. Mice that had been fasted for 16 h were injected with 100 μl normal saline (0.9% NaCl), with or without 10 units/kg body wt of insulin via the tail vein. Hindlimb muscles were removed 300 s later and immediately homogenized. After centrifugation, the resulting supernatants were used for immunoprecipitation with anti–insulin receptor substrate 1 (IRS-1) antibody (17). Immunoprecipitates were subjected to SDS-PAGE and then immunoblotted using antiphosphotyrosine antibody (4G10) as described previously (17).

Blood analysis. Blood glucose, plasma insulin, leptin, adiponectin, tumor necrosis factor (TNF)-α, total cholesterol, triglyceride, and free fatty acid (FFA) concentrations were determined as described previously (4). Plasma lipoproteins were analyzed by high-performance liquid chromatography (HPLC) using molecular sieve columns (Skylight Biotech, Akita, Japan) (18).

Glucose and insulin tolerance tests. Glucose and insulin tolerance tests were performed as described previously with slight modification (19). Glucose tolerance tests were performed on fasted (10 h) mice. Mice were given oral glucose (1 g/kg body wt), and blood glucose was assayed immediately before and at 15, 30, 60, and 120 min postadministration. Insulin tolerance tests were performed on fed mice. Mice were injected with human regular insulin (1.5 units/kg body wt; Eli Lilly, Kobe, Japan) into the intraperitoneal space, and blood glucose was assayed immediately before and at 20, 40, 60, and 80 min postinjection.

Hyperinsulinemic-euglycemic clamp. Hyperinsulinemic-euglycemic clamp studies were performed as described previously (20). Chronically cannulated, conscious and unrestrained mice were fasted for 6 h before the study. Insulin (500 $mU \cdot kg^{-1} \cdot min^{-1}$) was infused throughout the clamp study. Blood glucose was monitored every 5 min via carotid arterial catheter samples. Glucose was infused at a variable rate to maintain blood glucose at 120 mg/dl. The glucose infusion rate and endogenous glucose production were calculated as described (20).

Quantitative RT-PCR–based gene expression. Total RNA was isolated from 0.1 g mouse adipose tissue with Isogen (Wako Pure Chemical, Osaka, Japan), and cDNA was synthesized with a Cloned AMV First Strand Synthesis Kit (Invitrogen, Rockville, MD) using 5 μg total RNA. cDNA synthesized from total RNA was evaluated using real-time quantitative PCR (Light Cycler Quick System 350S; Roche Diagnostics, Mannheim, Germany). The relative amount of mRNA was calculated with 28S rRNA as the invariant control. The primers used are described in Supplemental Table 1 (online appendix [available at http://diabetes.diabetesjournals.org]).

β-VLDL uptake into cultured adipocytes. Murine 3T3-L1 preadipocytes were maintained and differentiated into adipocytes as described previously (21). β-VLDL ($d < 1.006$ g/ml) was purified from the blood of $apoE^{-/-}$ mice with high-fat loading and labeled with fluorescent lipid DiI (1,1′-dioctadecyl-3,3,3′,3′-tetramethylindocarbocyanine perchlorate) as described previously (22). After labeling with DiI, β-VLDL was incubated with an equal amount of recombinant human apoE3 for 1 h at 37°C (23). DiI-labeled β-VLDL (4 μg protein/ml) with or without apoE had been incubated with fully differentiated 3T3-L1 adipocytes for 8 h at 37°C. Cells were rinsed twice with PBS and solubilized with 0.1 N NaOH/1% SDS. Fluorescent intensities of cell lysates were measured with a fluorescent spectrophotometer (F-2000; Hitachi, Tokyo, Japan) (24).

Triglyceride secretion rate. To assess hepatic triglyceride secretion, 500 mg/kg Triton WR-1339 (Sigma), which blocks lipolysis of triglycerides in peripheral tissue, was injected into the tail veins of the 6 h–fasted $apoE^{+/+}$; Ay/+ mice, and blood samples were taken immediately before and 30, 60, and 90 min after injection (25).

Hepatic uptake of β-VLDL. Male C57BL/6N mice at 6 weeks of age were injected via tail vein with fluorescent β-VLDL (5 μg/mouse) with or without apoE in 0.2 ml PBS. Thirty minutes after injection, the mice were killed and their livers excised for lipid extraction and fluorescence measurement as described previously (26).

Statistical analysis. All data were expressed as means ± SEM. The statistical significance of differences was assessed by the unpaired *t* test and one-factor ANOVA.

RESULTS

ApoE deficiency inhibited the development of obesity. This study was prompted by the unexpected observation that aged $apoE^{-/-}$ mice are leaner and more insulin sensitive than $apoE^{+/+}$ mice of the same age with the C57BL/6J background. Therefore, we weighed $apoE^{-/-}$ and $apoE^{+/+}$ mice from 6 to 42 weeks of age, while maintaining the animals on high-fat chow. Body weights were similar through 10 weeks of age, but $apoE^{-/-}$ mice had significantly lower body weights after 14 weeks of age (Fig. 1*A*). Glucose tolerance in 30-week-old $apoE^{-/-}$ mice was moderately better than that in $apoE^{+/+}$ littermate mice (Fig. 1*B*). Thus, apoE deficiency prevents the development of obesity and associated glucose intolerance, while its effects on glucose tolerance are small.

Next, to elucidate the roles of apoE in development of the metabolic disorders associated with obesity, we established $apoE^{+/+}$;Ay/+, $apoE^{+/-}$;Ay/+, and $apoE^{-/-}$;Ay/+ mice. These mice were fed a 15% fat chow from 6 weeks of age. First, we compared body weights. As shown in Fig. 1*C*, mice gained weight in an apoE gene dosage-dependent manner; apoE deficiency significantly suppressed weight gain. Several organs and tissues were weighed at 11 weeks of age. Weights of the liver and both brown and white adipose tissues were significantly lower in an apoE gene dosage-dependent manner (Fig. 1*D*). In contrast, weights of other organs, which are minimally involved in lipid accumulation, were similar in $apoE^{+/+}$;Ay/+ and $apoE^{-/-}$; Ay/+ mice (Supplemental Table 2 [online appendix]). Triglyceride contents of the liver and mesenteric adipose

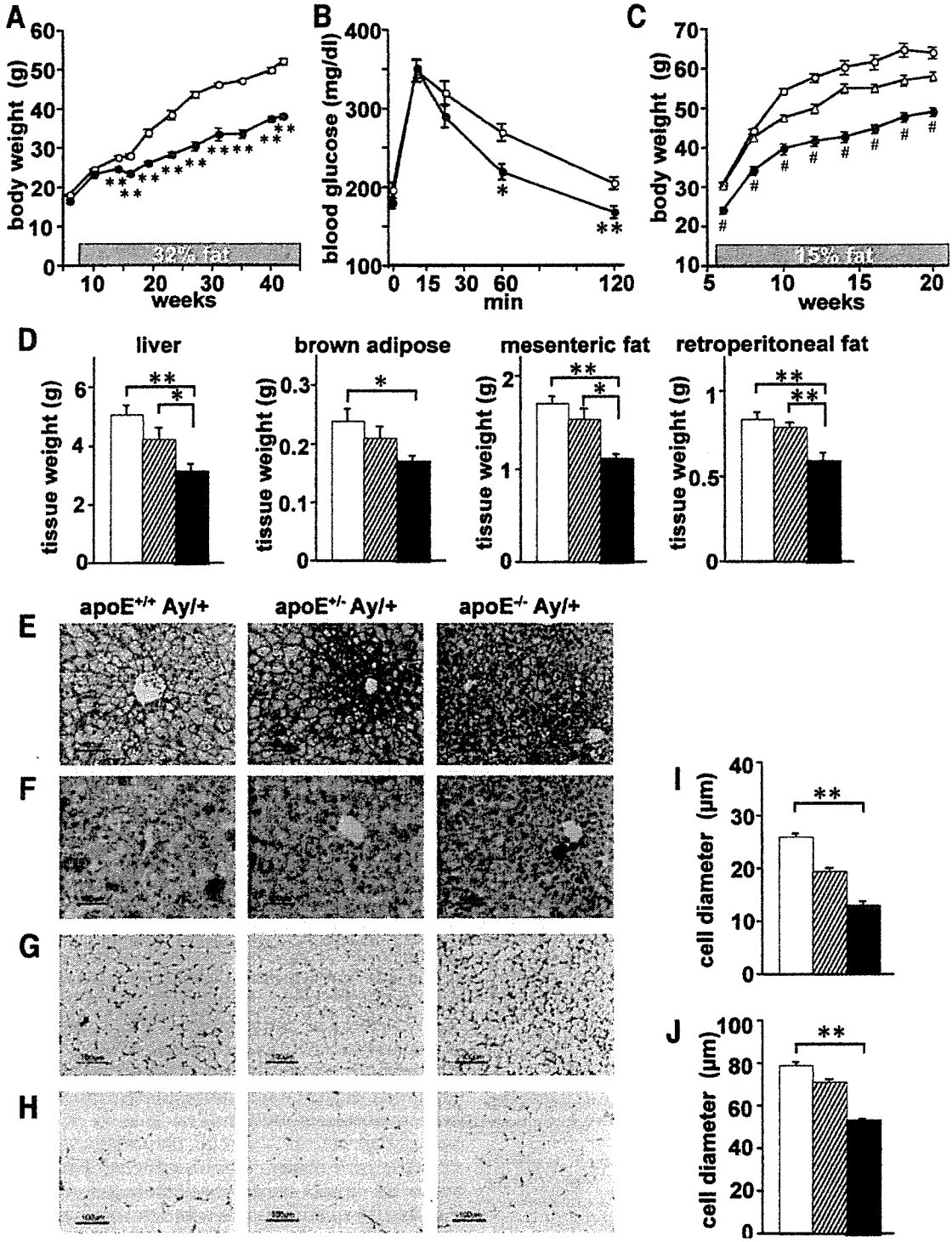

FIG. 1. ApoE deficiency suppressed body weight gain and fat accumulation. *A* and *B*: Body weights were determined from 6 to 40 weeks of age (*A*) and glucose tolerance tests were performed (*B*) in apoE$^{+/+}$ mice (○) and apoE$^{-/-}$ mice (●; n = 6 per group) at 30 weeks of age with the C57BL/6 background. *C*: Body weights were determined from 6 to 20 weeks of age in apoE$^{+/+}$;Ay/+ (○), apoE$^{+/-}$;Ay/+ (△), and apoE$^{-/-}$;Ay/+ (●) mice fed 15% fat chow. *D–J*: The liver and fat tissues of apoE$^{+/+}$;Ay/+, apoE$^{+/-}$;Ay/+, and apoE$^{-/-}$;Ay/+ mice at 11 weeks of age. *D*: The liver, brown adipose, and mesenteric and retroperitoneal white adipose tissues from apoE$^{+/+}$;Ay/+ (□), apoE$^{+/-}$;Ay/+ (▨), and apoE$^{-/-}$;Ay/+ (■) mice (n = 6–8 per group) were weighed. *E–J*: Histological findings of the liver stained with hematoxylin-eosin (*E*) and Oil Red O (*F*), as well as hematoxylin-eosin staining of brown adipose (*G*) and mesenteric white adipose (*H*) tissues in apoE$^{+/+}$;Ay/+ (*left*), apoE$^{+/-}$;Ay/+ (*middle*), and apoE$^{-/-}$;Ay/+ (*right*) mice. Brown adipose (*I*) and mesenteric white adipose (*J*) cell diameters were measured in apoE$^{+/+}$;Ay/+ (□), apoE$^{+/-}$;Ay/+ (▨), and apoE$^{-/-}$;Ay/+ (□) mice. Representative histological findings are shown. Data are presented as means ± SE. *P < 0.05, **P < 0.01 by the unpaired t test and one-way ANOVA.

tissue were significantly smaller in apoE$^{-/-}$;Ay/+ than in apoE$^{+/+}$;Ay/+ mice (apoE$^{+/+}$;Ay/+ vs. apoE$^{-/-}$;Ay/+ mice: liver, 0.467 ± 0.069 vs. 0.365 ± 0.036 mg/protein, P = 0.02; white adipose tissue, 12.4 ± 1.4 vs. 5.8 ± 1.3 mg/protein, P = 0.002). Histological analyses revealed that apoE deficiency inhibited hepatic fat accumulation, while abundant lipid droplets were present in the livers of apoE$^{+/+}$;Ay/+ mice (Fig. 1*E* and *F*). In addition, brown

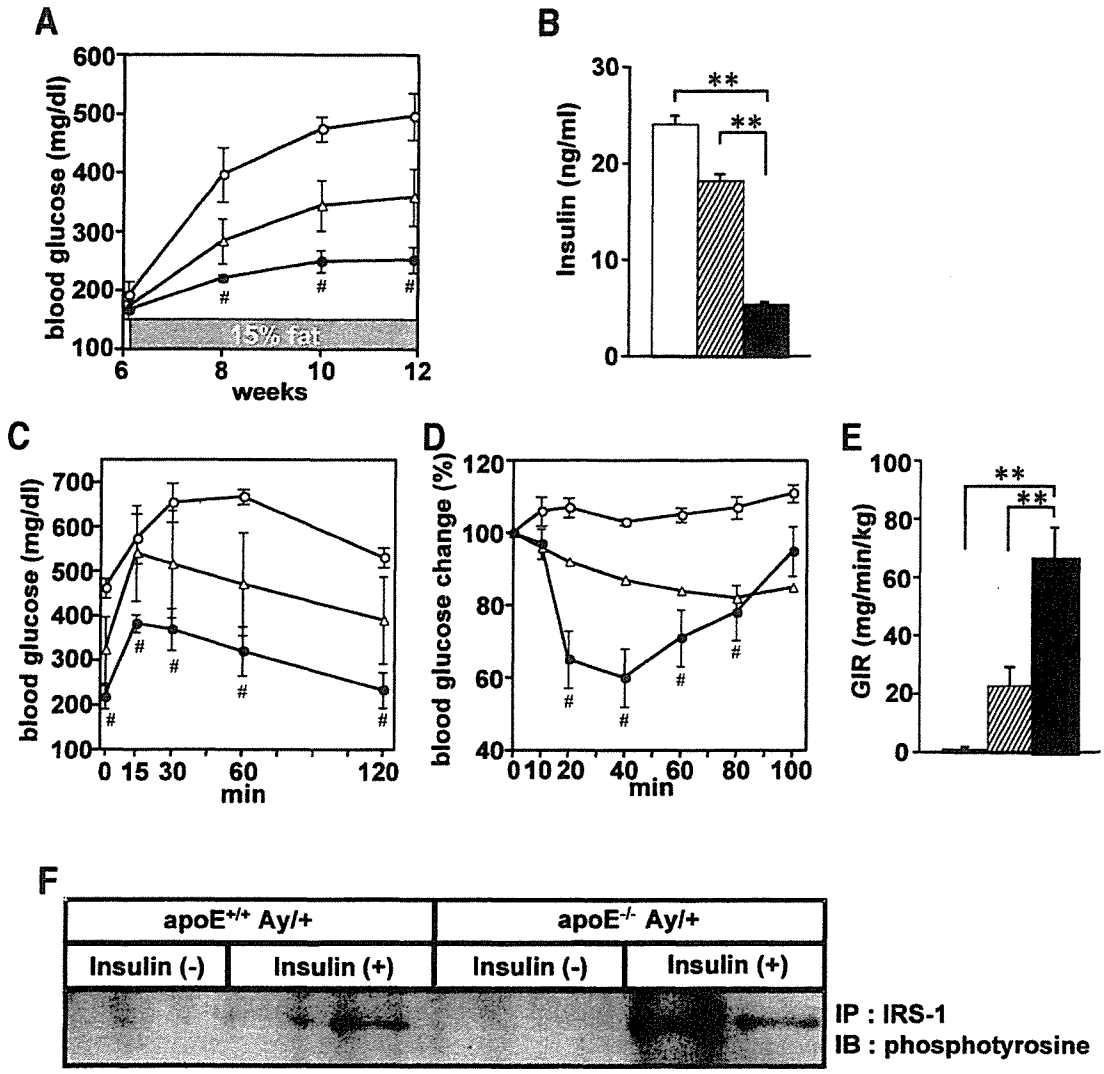

FIG. 2. ApoE deficiency improved glucose tolerance and insulin sensitivity in genetically obese mice. *A*: Fasting blood glucose levels were examined in apoE$^{+/+}$;Ay/+ (○), apoE$^{+/-}$;Ay/+ (△), and apoE$^{-/-}$;Ay/+ (●) mice biweekly from 6 to 12 weeks of age. *B*: Fasting plasma insulin levels of apoE$^{+/+}$;Ay/+ (□), apoE$^{+/-}$;Ay/+ (▨), and apoE$^{-/-}$;Ay/+ (■) mice were measured. *C* and *D*: Glucose tolerance (*C*) and insulin tolerance (*D*) tests were performed in apoE$^{+/+}$;Ay/+ (○), apoE$^{+/-}$;Ay/+ (△), and apoE$^{-/-}$;Ay/+ (●) mice. Data were expressed as percentages of blood glucose levels immediately before intraperitoneal insulin loading (n = 4–6 per group). *E*: Glucose infusion rates during hyperinsulinemic-euglycemic clamp studies were measured in apoE$^{+/+}$;Ay/+ (□), apoE$^{+/-}$;Ay/+ (▨), and apoE$^{-/-}$;Ay/+ (■) mice (n = 3 per group). *F*: Insulin-stimulated tyrosine phosphorylation of IRS-1 proteins in muscle. Mice that had been fasted for 16 h received an intravenous injection of 100 μl normal saline with or without insulin (10 units/kg body wt). Hindlimb muscles were removed 300 s later, and lysates were immunoprecipitated with anti–IRS-1 antibody. Immunoprecipitates were subjected to SDS-PAGE and immunoblotted with anti-phosphotyrosine antibody (4G10). Representative histological findings and immunoblots are presented. These metabolic studies in *B–F* were performed using 11-week-old mice. In *A–E*, data are presented graphically as means ± SE. *P < 0.05, **P < 0.01 by the unpaired t test and one-way ANOVA.

(Fig. 1*G*) and white (Fig. 1*H*) adipose tissues of apoE$^{-/-}$;Ay/+ mice were significantly smaller than those of apoE$^{+/+}$;Ay/+ mice. ApoE deficiency also decreased cell diameters in both brown (Fig. 1*I*) and white (Fig. 1*J*) adipose tissues. These findings suggest that apoE deficiency results in resistance to obesity via suppression of fat accumulation in the liver and fat tissues under obesity-inducing conditions.

ApoE deficiency induced greater glucose tolerance and insulin sensitivity in obese states. As described previously (15), lipid metabolism was markedly impaired with apoE deficiency (Supplemental Fig. 1*A* [online appendix]). Plasma cholesterol, triglyceride, and FFA levels were markedly higher in apoE$^{-/-}$;Ay/+ than in apoE$^{+/+}$;Ay/+ mice. HPLC analysis of plasma lipid profiles revealed that chylomicron, VLDL, and LDL fractions were markedly increased in apoE$^{-/-}$;Ay/+ compared with apoE$^{+/+}$;Ay/+ mice (Supplemental Fig. 1*B* [online appendix]).

Next, we examined the effects of apoE deficiency on glucose metabolism as well as insulin sensitivity in genetically obese Ay mice. From age 8 weeks onward, fasting blood glucose was markedly increased in apoE$^{+/+}$;Ay/+ mice on high-fat chow, but this glucose elevation was significantly inhibited by apoE deficiency (Fig. 2*A*). Fasting blood insulin levels at 11 weeks of age were lower, by 78%, in apoE$^{-/-}$;Ay/+ than in apoE$^{+/+}$;Ay/+ mice (Fig. 2*B*). Glucose (Fig. 2*C*) and insulin (Fig. 2*D*) tolerance tests documented that ApoE$^{-/-}$;Ay/+ mice were more glucose tolerant and insulin sensitive. We further examined insulin sensitivity using hyperinsulinemic-euglycemic clamp procedures. ApoE$^{+/+}$;Ay/+ mice fed high-fat chow exhibited severe insulin resistance, while in apoE$^{-/-}$;Ay/+ mice, glucose infusion rates were markedly higher, by 54-fold (Fig. 2*E*). Thus, despite hyperlipidemia, especially increased plasma FFA levels, apoE deficiency markedly

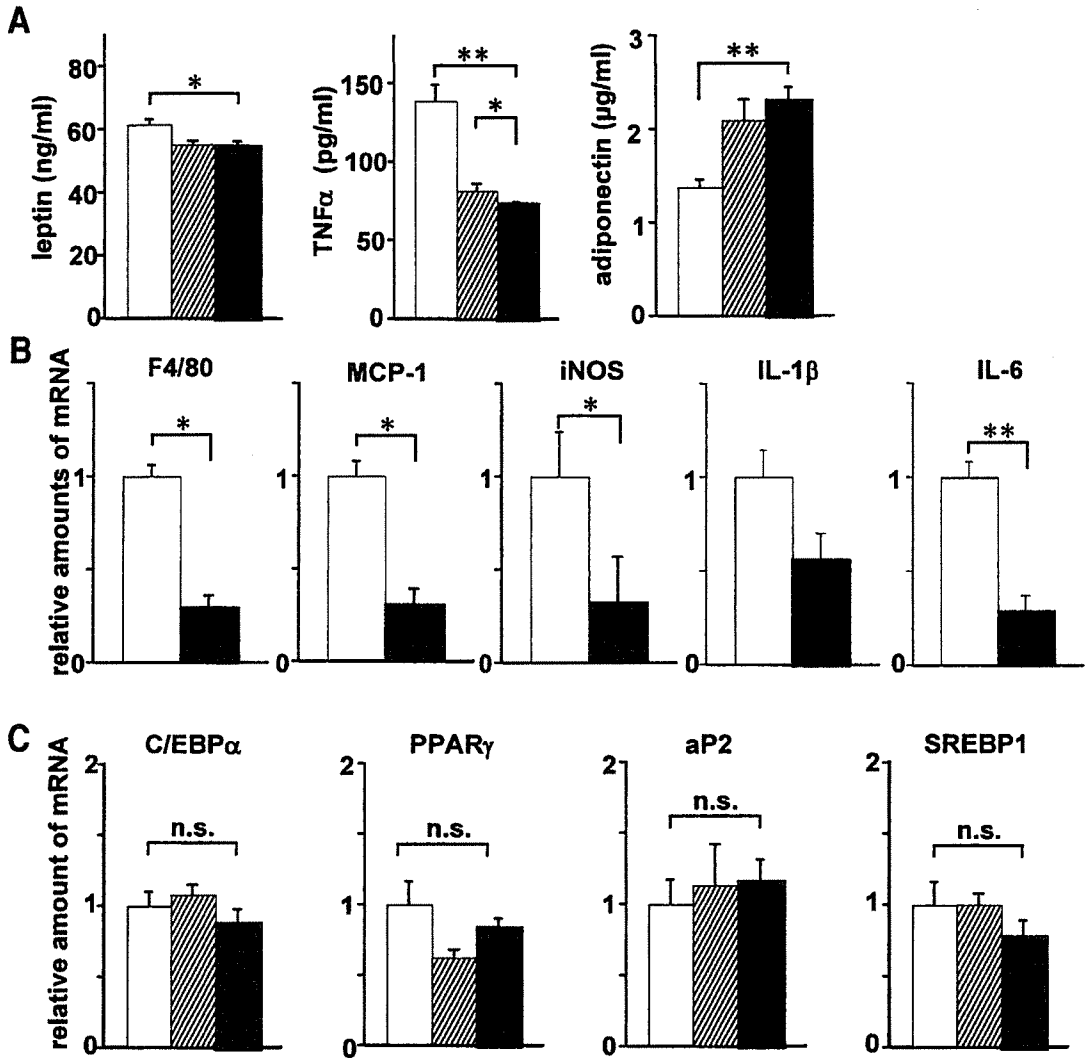

FIG. 3. ApoE deficiency affected plasma adipocytokine profiles and expressions of the mRNAs for inflammation- and differentiation-related proteins in adipose tissue. *A*: Plasma adipocytokines (*left*, leptin; *middle*, TNF-α; *right*, adiponectin) of high-fat chow–fed apoE$^{+/+}$;Ay/+ (□), apoE$^{+/-}$;Ay/+ (▨), and apoE$^{-/-}$;Ay/+ (■) mice were measured after a 10-h fast at 11 weeks of age. *B* and *C*: Relative amounts of mRNA in mesenteric white adipose tissue from apoE$^{+/+}$;Ay/+ (□) and apoE$^{-/-}$;Ay/+ (■) mice were determined by quantitative RT-PCR and corrected with 28S rRNA as the internal standard. Total RNA in white adipose tissue was isolated, after a 10-h fast, from 11-week-old mice. Levels of the mRNA levels for inflammation (*B*)- and differentiation (*C*)-related proteins in adipose tissue were assayed (n = 6 per group). Data are presented as means ± SE. *P < 0.05, **P < 0.01 by one-way ANOVA (*A*) and the unpaired t test (*B* and *C*).

improves glucose tolerance and insulin sensitivity. In addition, insulin-stimulated tyrosine phosphorylation of IRS-1 in muscle was enhanced in apoE$^{-/-}$;Ay/+ compared with apoE$^{+/+}$;Ay/+ mice (Fig. 2*F*). Thus, apoE deficiency apparently prevents surplus fat accumulation in adipose tissue and insulin resistance in muscle, resulting in better glucose tolerance.

Adipocytes are differentiated normally in apoE$^{-/-}$;Ay/+ mice in vivo. We next determined plasma adipocytokine profiles (Fig. 3*A*). In apoE$^{-/-}$;Ay/+ mice, plasma leptin levels were slightly decreased and TNF-α levels were markedly lower than those in apoE$^{+/+}$;Ay/+ mice, while plasma adiponectin levels were significantly higher. Thus, apoE deficiency improved obesity-induced alterations in adipocytokine profiles. In addition, quantitative RT-PCR revealed that expressions of F4/80, monocyte chemoattractant protein-1, inducible nitric oxide synthase, and interleukin-6 in mesenteric adipose tissue were significantly lower in apoE$^{-/-}$;Ay/+ than in apoE$^{+/+}$;Ay/+ mice (Fig. 3*B*), suggesting inhibition of inflammation and macrophage invasion into adipose tissue. Obesity is reportedly associated with macrophage infiltration of adipose tissue, which is likely to promote insulin resistance (27,28). Inhibition of macrophage invasion of adipose tissue may be involved in the higher insulin sensitivity and glucose tolerance observed in apoE$^{-/-}$;Ay/+ mice.

As described above, plasma adiponectin levels were increased in apoE$^{-/-}$;Ay/+ mice, suggesting normal adipocyte differentiation in vivo. Furthermore, mRNA expressions for adipocyte-related proteins, such as CCAAT/enhancer binding protein-α, peroxisome proliferator–activated receptor-γ, and aP2, were similar among adipose tissues from apoE$^{+/+}$;Ay/+, apoE$^{+/-}$;Ay/+, and apoE$^{-/-}$;Ay/+ mice (Fig. 3*C*). mRNA expressions levels of these three genes were also similar in adipose tissues from younger apoE$^{+/+}$;Ay/+ and apoE$^{-/-}$;Ay/+ mice, 4 weeks of age, when body weights were not significantly different (data not shown). In addition, apoE deficiency did not alter sterol regulatory element–binding protein 1 (SREBP1) expression (Fig. 3*C*). These findings indicate